Science Bulletin 69 (2024) 1515–1535

Contents lists available at ScienceDirect

Science Bulletin

journal homepage: www.elsevier.com/locate/scib

Review

Rydberg atom electric field sensing for metrology, communication and hybrid quantum systems

Hao Zhang [a,b,1], Yu Ma [c,1], Kaiyu Liao [d,1], Wenguang Yang [a,b], Zongkai Liu [c], Dongsheng Ding [c,*], Hui Yan [d,f,*], Wenhui Li [e,*], Linjie Zhang [a,b,f,*]

[a] State Key Laboratory of Quantum Optics and Quantum Optics Devices, Institute of Laser Spectroscopy, Shanxi University, Taiyuan 030006, China
[b] Collaborative Innovation Center of Extreme Optics, Shanxi University, Taiyuan 030006, China
[c] CAS Key Laboratory of Quantum Information, University of Science and Technology of China, Hefei 230036, China
[d] Key Laboratory of Atomic and Subatomic Structure and Quantum Control (Ministry of Education), Guangdong Basic Research Center of Excellence for Structure and Fundamental Interactions of Matter, School of Physics, South China Normal University, Guangzhou 510006, China
[e] Centre for Quantum Technologies, National University of Singapore, Singapore 117543, Singapore
[f] Hefei National Laboratory, Hefei 230088, China

ARTICLE INFO

Article history:
Received 13 November 2023
Received in revised form 29 January 2024
Accepted 11 March 2024
Available online 19 March 2024

Keywords:
Rydberg atom
Electric field sensing
Atomic sensor

ABSTRACT

Rydberg atoms-based electric field sensing has developed rapidly over the past decade. A variety of theoretical proposals and experiment configurations are suggested and realized to improve the measurement metrics, such as intensity sensitivity, bandwidth, phase, and accuracy. The Stark effect and electromagnetically induced transparency (EIT) or electromagnetically induced absorption (EIA) are fundamental physics principles behind the stage. Furthermore, various techniques such as amplitude- or frequency-modulation, optical homodyne read-out, microwave superheterodyne and frequency conversion based on multi-wave mixing in atoms are utilized to push the metrics into higher levels. In this review, different technologies and the corresponding metrics they had achieved were presented, hoping to inspire more possibilities in the improvement of metrics of Rydberg atom-based electric field sensing and broadness of application scenarios.

1. Introduction

Electromagnetic (EM) waves are the cornerstone of modern science and technology, exerting a profoundly significant influence on various fields. The propagation characteristics of EM waves and their principles of interaction with matter are utilized in various application scenarios such as communications, remote sensing, radar detection, medical and healthcare, defense and military applications. Electric fields and magnetic fields are distinct due to the different nature of their interactions with matter, which are the Coulomb potential of electric field and Lorentz force of the magnetic field. The strength of magnetic interaction is different from that of electric interaction by a factor of v/c, where v and c are the speeds of charged particle and light, respectively. Normally, $v \ll c$ means that interactions of charged particles with magnetic fields are much weaker than that with electric fields [1]. Considering the interactions between EM waves and charged particles, generally, we focus on the electric component of EM waves, of which the detection and sensing provide possibilities for various applications.

Since the pioneer work conducted by Hertz [2], who used a dipole antenna to prove the existence of EM waves by both transmitting and receiving, the development of tools for transmitting and receiving EM waves mainly focused on an antenna. Different types of antennas gradually emerged and adapted for various application scenarios considering their optimal working conditions. Such as resonant antennas for which EM waves travel back and forth in between the structure of the antenna, and off-resonant ones which allow the traveling wave to propagate. Another type of antenna which is also often seen is aperture antenna [3]. The scheme of these conventional antenna is when microwave radiation impinges on the antenna, it induces electrical currents within the antenna's conductive elements. This absorption of microwave energy generates an electrical voltage or current

* Corresponding authors.
E-mail addresses: dds@ustc.edu.cn (D. Ding), yanhui@scnu.edu.cn (H. Yan), wenhui.li@nus.edu.sg (W. Li), zlj@sxu.edu.cn (L. Zhang).
[1] These authors contributed equally to this work.

https://doi.org/10.1016/j.scib.2024.03.032

in the antenna. Over the years, there has not been a significant change in these basic concepts of how antennas receive microwave signals. However, there are some inherent flaws of the traditional metal antennas.

Low sensitivity The current formed by the directional motion of charge carriers induced by antenna absorption of EM waves is the physical basis for microwave antenna measurements. According to the Johnson-Nyquist theorem, the electronic noise was generated by the thermal agitation of the charge carriers (usually the electrons) inside an electrical conductor at equilibrium, which happens regardless of any applied voltage [4,5]. Normally at room temperature, that is 300 K, and in the bandwidth of 1 Hz, the thermal noise power is −174 dBm.

Limited bandwidth Due to the optimal response of the antenna to EM waves, the size effects should be considered. In general, the size of an antenna is inversely proportional to the frequency of the EM waves it receives or transmits. Especially for small antennas of which the receiving bandwidth is normally low, according to the Chu-Harriton limit, the lower limit for a lossless linear polarized antenna is [6–8]

$$Q \geqslant \frac{1}{k^3a^3}+\frac{1}{ka}, \tag{1}$$

where $k = 2\pi/\lambda$ is wavenumber and a is characteristic length of the antenna. As antennas are made smaller, the bandwidth shrinks and radiation resistance becomes smaller compared to loss resistances that may be present, thus reducing the radiation efficiency.

Electric field distortion When the detection antenna is placed near the radiation source, the distortion of the target EM waves could be induced via the coupling between the measured electric field and the detecting antenna and non-uniformity of the electric field caused by the detecting antenna.

Inadequate accuracy At present, the intensity standards of the electric component of EM waves rely on the standard antenna which is calibrated via standard electric fields. This chicken-egg dilemma sets the intrinsic uncertainty for the measurement precision of the electric field of EM waves. This becomes a giant barrier for setting up the standards for the very strong electric field which is over several kV/cm.

As mentioned above, conventional methods for measuring the electric field of EM waves based on metal antenna encounter a development bottleneck as the sensitivities, bandwidth, and precision are limited. In 2018, the International General Conference on Weights and Measures announced that all seven of the international basic units have been traced back to physical constants, marking the entry of metrology into the quantum era. Atoms have provided ideal platforms for setting up the quantum standards for various physical parameters. One of the most notable development is that with the help of state of art laser techniques, the fractional frequency measurement uncertainty in the atomic sample of ultracold strontium is reaching 7.6×10^{-21} at present [9]. An ultrasensitive atomic magnetometer was realized based on optically pumped potassium atoms operating in a spin-exchange relaxation-free regime. The demonstrated magnetic field sensitivity of 160 aT/Hz$^{1/2}$ is achieved [10].

In recent years, research on electric field measurements of EM waves based on atomic sensors has gradually attracted attention, and a substantial amount of related investigations has emerged. The research primarily focuses on quantum measurements of microwave field using Rydberg atoms. Rydberg atoms refer to the atoms that are excited to bound states which possess higher energy marked with larger principal quantum number n. These atoms are named after the Swedish scientist J. R. Rydberg who formulated the following equation to describe the relations between radiation energies and atomic structures:

$$\nu = R\left(\frac{1}{n^2}-\frac{1}{n'^2}\right), \tag{2}$$

where ν is the wavenumber of radiation, and R is called Rydberg constant which is 10 973 731.568 160(21) m^{-1} [11]. Here n and n' are the principal quantum number of initial and final states, respectively. For alkali atoms, the energies of states with low angular momentum quantum numbers, such as s, p, d states would decrease compared to their hydrogen counterpart which is quantified with quantum defect $\delta_l(n)$. It is dependent both on n and angular momentum l, and would be clarified semi-empirically by the Rydberg-Ritz formula:

$$\delta^l(n) = \delta_0^l + \frac{\delta_2^l}{\left(n-\delta_0^l\right)^2} + \frac{\delta_4^l}{\left(n-\delta_4^l\right)^4} + \ldots \tag{3}$$

then the corrected form of the Rydberg formula for alkali atoms would become

$$\nu_{n,n'} = R_A\left(\frac{1}{\left[n-\delta^l(n)\right]^2}-\frac{1}{\left[n'-\delta^l(n')\right]^2}\right). \tag{4}$$

Compared to ground state atoms, Rydberg atoms exhibit extremely exaggerated properties. All of these properties have different scaling dependence on n which need both numerical calculation in the basis of Rydberg wavefunctions as shown in Fig. 1 and scaling of Rydberg energies. The intrinsically large electric dipoles of Rydberg atoms stem from the large distance that the outer-most electron is away from the inner positive ionic core, the strength of which scales as n^2. The polarizabilities of certain energies become significantly large as they are n^7 dependence, making the Rydberg atoms easily perturbed by the external electric field, and hence highly sensitive sensors for perception of electric component of EM waves.

Energy gaps between Rydberg states scale as n^{-3}. The precise and efficient preparation of a specific Rydberg state requires narrow energy distribution over frequency of excitation. The invention of the laser provided an ideal tool for the investigations of Rydberg atoms. After the state preparation, the detection of Rydberg atoms is also an issue. The state-selective-field-ionization (SSFI) detection methods are very effective since the energies of the Rydberg state are close to the ionization threshold. The atoms in different Rydberg states would be distinguished via time-of-flight (TOF) spectroscopy [13,14]. The dipole blockade induced by strong long-range interactions of Rydberg atoms [15–17] and states mixing

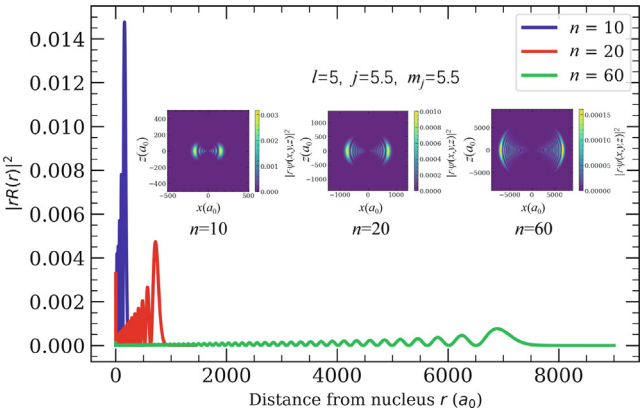

Fig. 1. (Color online) Radial wavefunctions of cesium with principal quantum number $n = 10, 20, 60$, $l = 5$; $j = 5.5$, and $m_j = 5.5$. The inset is projection of wavefunction on the plane of x-z. The wavefunctions are calculated based on the Alkali-Rydberg-Calculator (ARC) package [12].

effect [18–20] are investigated in cold Rydberg atoms with help of SSFI technique.

Although the SSFI detection method is efficient and directly measures the number of Rydberg atoms, the atoms are broken down into ions and electrons which means that it is a destructive way of detection. With the development of quantum optics, electromagnetically induced transparency (EIT) was first experimentally realized in 1991 [21] soon after its theoretical proposal by the same group in 1990 [22]. EIT is a quantum optical phenomenon that occurs when a medium, typically an atomic or molecular gas, becomes transparent to a probe laser beam due to the interaction with a control laser field. In an EIT system, the control laser field modifies the energy levels and transitions of the atoms or molecules in such a way that it cancels the absorption of the probe laser at a specific frequency, making the medium transparent at that frequency. It is specific to medium with large optical depth (OD) in which both laser and medium states are modified [23]. For Rydberg atoms, considering two-photon excitation, the coherence exists between two coupled transitions consisting of a ground state and a Rydberg state sharing a common intermediate state. EIT phenomenon was utilized for coherent full optical detection of Rydberg states [24,25], which is most importantly a non-destructive method and is preferable in the application of quantum information and precision measurement. Various fundamental physics and experimental techniques related to Rydberg physics, utilizing EIT as a detection method, have been proposed and implemented by researchers. By coupling a probe transition to a Rydberg state using EIT, the strong dipole–dipole interactions were mapped onto an optical field [26]. The optical photons could be stored in highly excited collective states (Rydberg polaritons) enabling both fast qubit rotations and control of photon-photon interactions [27]. The laser frequencies which are not related to any obvious absorption spectra can be stabilized with the help of EIT by modulation transfer technique [28,29].

Due to large transition dipole moments between nearby Rydberg states, the population transfer between Rydberg states could be effectively controlled, and strong resonant dipole–dipole interactions [30] or off-resonant van de Waals interactions [31] can be precisely tuned. Microwave spectroscopy based on two-photon transition was also employed for the precision measurement of quantum defects of ns, np, nd [32], nf [33] and ng [34] Rydberg states of rubidium. Besides alkali-metal atoms, millimeter-wave transitions between molecular Rydberg states ($n \sim 35$) of BF molecules were also observed with Chirped-Pulse millimeter-Wave spectroscopy [35]. EIT spectroscopy has been an effective and basic tool in the precision measurement of the electric field of EM waves and metrology. In this review, different measurement methods of an electric field based on Rydberg atoms are presented, including the Stark effect which could be used for electric field sensing in low frequency regime and continuous frequency detunings. The conventional AT splitting induced by microwave and recently developed atomic superheterodyne techniques are introduced in detail. Three novel approaches based on frequency conversion and frequency comb and non-equilibrium state sensing are presented to provide new opportunities for improvement of sensitivity and bandwidth of atomic electric field sensors. As shown in Fig. 2, the methods for electric field sensing based on Rydberg atoms are summarized with sensitivity, working bandwidth and instantaneous bandwidth as indicators. A comparison between different schemes of electric sensing including conventional metal antenna, Rydberg atoms, trapped ions, and electric-optical crystals is presented. The sensitivity of conventional metal antenna is calculated with a sensing area comparable with that of an atomic sensor which is around 1 cm^2. At last, application development is given in the categories of metrology, communication and imaging (see Table 1).

2. Stark shift

2.1. Principle

Due to the large polarizability of Rydberg atoms, energies of these high-lying states are very sensitive to the external electric field, and exhibit obvious energies shift or splitting which is known as the Stark effect. From the second-order perturbation theory, the Stark shift of Rydberg atoms under an electric field is

$$\Delta E = -\frac{1}{2}\alpha E^2, \tag{5}$$

where α is the polarizability which in principle includes scalar and tensor parts, ΔE is energy shift of the certain Rydberg state, and E is the electric field. As shown in Fig. 3a, the stark map of Cesium in the

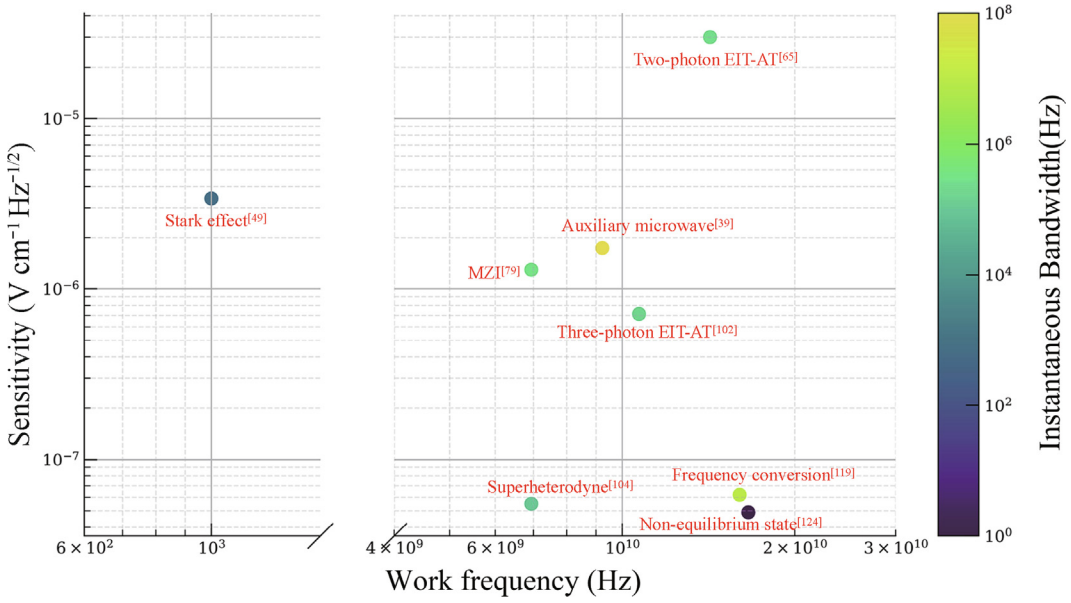

Fig. 2. (Color online) Comparison of different schemes of electric field sensing based on Rydberg atoms. The sensitivity, working bandwidth and instantaneous bandwidth are considered as indicators to illustrate the pros and cons of these methods.

Table 1
Comparison between different schemes for electric field sensing.

System	Mechanism	Working bandwidth	Sensitivity	Instantaneous bandwidth
Metal antenna	Carrier motion	MHz – THz [36]	1.5 nV cm^{-1} Hz$^{-1/2}$ [4]	~ 10 GHz [36]
Rydberg atoms	Quantum interference	DC – THz [37]	< nV cm^{-1} Hz$^{-1/2}$ [38]	~ 100 MHz [39]
Trapped ions	Force	DC – MHz [40]	500 nV cm^{-1} Hz$^{-1/2}$ [40]	~ MHz [40]
Electric-optical crystals	Electric-optical effect	DC – GHz [41]	10 μV cm^{-1} Hz$^{-1/2}$ [42]	~ GHz [41]

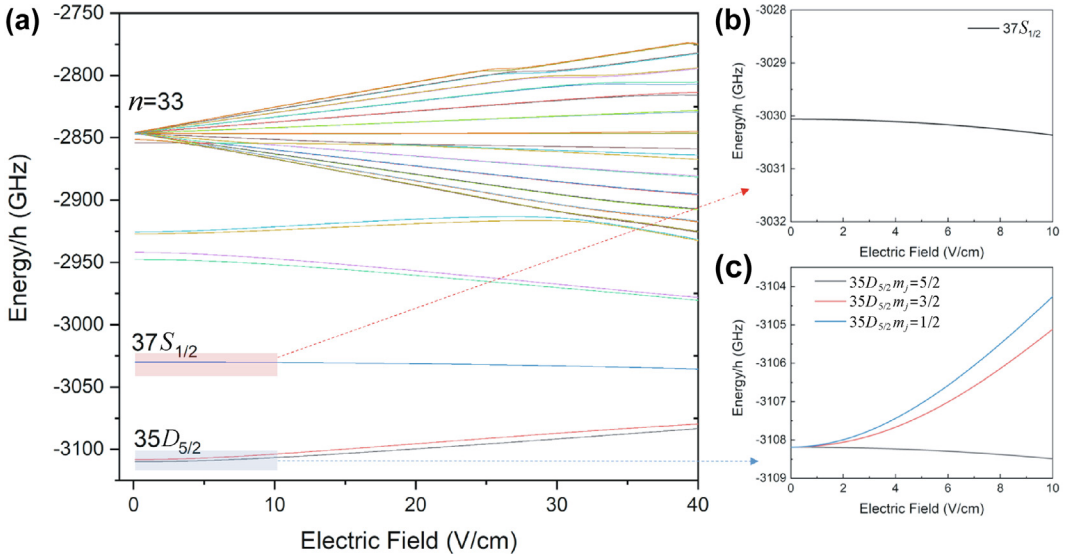

Fig. 3. (Color online) Stark map of Cesium atoms for $n = 33$. (a) Stark levels manifold in the vicinity of $n = 33$; (b) Stark level shift of Rydberg state of $37S_{1/2}$ of Cesium; (c) Stark levels splitting and shift of Rydberg state of $35D_{5/2}$ of Cesium atom. Calculated based on the ARC package [12].

vicinity of $n = 33$ is depicted. It is clear to see that states with angular momentum $l > 4$ constitute the $n = 33$ stark manifolds beside which $37S_{1/2}$ and $35D_{5/2}$ states of cesium also exist, as the quantum defects of S and D states are around 4 and 2. The $37S_{1/2}$ state exhibits merely level shift as S state possesses only magnetic states of $|m_j| = 1/2$ as shown in Fig. 3b, and $35D_{5/2}$ state shows not only levels shift but also energies splitting due to different polarizabilities of three $|m_j|$ states as shown in Fig. 3c. The Stark effects of Rydberg energies could be exploited for measuring the fundamental properties of Rydberg atoms. The polarizabilities of cesium nD [43] and nS [44] states are precisely measured. Apart from the measurement of fundamental parameters, it is straightforward to measure the DC electric field with relatively weak intensity. As shown in the results of the experiment conducted in 1999 [45], high Rydberg states of the krypton atom have been investigated at high resolution by vacuum ultraviolet–millimeter wave double-resonance spectroscopy. The measurement of Stark shifts in the spectra of these high Rydberg states is used to determine electric fields with a ± 20 μV cm^{-1} accuracy. Since the polarizabilities of Rydberg states are very large compared to the ground state, the second-order perturbation theory would be invalid at a relatively strong electric field, and the calculations of Stark shift should be carried out in the eigenstates set of $|J, m_J>$ [46]. The quadratic dependence of Stark shift on electric field strength as shown with Eq. (5) makes it insensitive to very small electric field signals. For single field measurement the sensitivity for intensity measurement is limited. An alternative way was exploited to increase the sensitivity which will be discussed in the following part. Besides DC electric field sensing, EM waves at low frequencies less than hundreds of MHz which are generally far off-resonant with neighbouring Rydberg transitions could be measured via the Stark effect.

2.2. Free charges

Considering the application feasibility, normally the atoms in room-temperature vapor cells are used for the EM wave measurement. The materials for vapor cell manufacture are generally good electric insulators, such as quartz, borosilicate, and sapphire. From a positive perspective, the disturbances to the electric fields of these non-metal materials are much less than those of metals. On the other side, there are some unique phenomenons connected to the intrinsic properties of dielectric materials. Because of the adsorption of alkali atoms on the non-metallic surfaces, the inner surface of a vapor cell can have nonzero conductivity [47]. This phenomenon leads to either the generation of an electric field inside the vapor cell without and in-built metal structure [48], or screening the DC or low frequency EM waves applied from outside of the vapor cell [49].

Due to the adsorption of atomic layers on the inner surface of the vapor cell, free charges can be induced by heating and laser illumination, which are attributed to Seeback [50] and photoelectric [51] effects. Besides the free charges inside the alkali atomic layers on the inner surface, volume free charges could also be originated from Rydberg atoms by blackbody or laser induced photoionization or collision process [52,53]. In the case where the fields generated inside the vapor cell could expressed as [54]

$$E = \frac{2.603e}{4\pi\varepsilon_0} \cdot N_C^{2/3}, \tag{6}$$

where E is the inhomogeneous electric field due to free volume charges, of which the density is N_C. The fields allow DC electric field tuning of up to 0.8 V cm^{-1} within the Rydberg EIT probe region [48]. The energy levels of nS Rydberg states of cesium atoms shifted

almost 900 MHz due to the generated electric fields [53]. Considering the screening effect, an empirical equation $E_i(t) = E_{ext}\exp(-t/1.5\epsilon R_{\square} r)$, where $E_i(t)$ is the total electric field inside the vapor cell, and E_{ext} is applied field externally, and $R_{\square}$ is the sheet resistance on the inner surface, and r is the characteristic length of the cell. The time for establishing the screening effect could scale up to the order of seconds on a rubidium-vapor cell that is made of monocrystalline sapphire. The cut-off frequency significantly decreases to the orders of kHz. The demonstrated sensitivity was around 0.34 mV m^{-1} Hz$^{-1/2}$ at a 3-dB low cutoff frequency of 770 Hz [49].

2.3. Strong field

As mentioned above, the quadratic behavior of Stark shift on the electric field strength is valid under weak field scenarios. In the strong field regime, the Rydberg levels exhibit higher-order couplings and state mixing with high-l states [55]. To describe this strong-field level modulation and states mixing phenomenon, Floquet theory should be applied for quantitative explanations [56–58]. For a time-periodic Hamiltonian $\widehat{H}(t) = \widehat{H}(t+T)$, where T is the period of EM waves, the wavefunction satisfying the Schrödinger's equation is

$$\Psi_v(t) = e^{-iW_v t/\hbar}\psi_v(t), \tag{7}$$

where W_v is energies for periodic Floquet modes ψ_v, which could be expanded with standard bare atomic states $|n,l,j,m_j> = |k>$

$$\Psi_v = e^{-iW_v t/\hbar}\sum_k C_{v,k}(t)|k> . \tag{8}$$

The Floquet states Ψ_v and its corresponding eigenenergies could be determined via diagonalizing the time-evolution operator $\widehat{U}(t, t+T)$ [58].

The Rydberg levels modulations at electric field strength up to 3.5 V cm^{-1} with frequency of 70 MHz [55], and 2.3 V cm^{-1} (uncertainties of 6%) at frequency of about 40 MHz [58], and 2.96 V cm^{-1} (uncertainties of 0.35%) with EM waves frequencies of 50 and 100 MHz [56] are measured experimentally. Near-field imaging of the radiation pattern of microwave at 13.49 GHz was mapped with resolution of $\sim\lambda/10$ and the field dynamical range of 72–240 V cm^{-1} with AC Stark shifts of single Rydberg resonance [59].

2.4. Hybrid atomic vapor cell

To address the electric field screening effect caused by non-metallic atomic vapor cells during the measurement of DC electric fields or low-frequency EM waves, various electrode structures have been designed and installed inside the chamber, creating hybrid atomic vapor cells. A split field-enhancement resonator embedded in a Rb vapor cell was employed to enhance and detect C-band radio-frequency (RF) fields. A gain of 24 dB has been achieved in the intensity sensitivity [60]. For the measurement of VHF-band RF fields, which is 50–500 MHz with up to 5 kV m^{-1} intensity, A vapor cell with integrated electrodes is used. Two planar steel electrodes separated by a narrow gap of about 400 μm are installed inside the vapor cell to produce electric fields exceeding 10 kV m^{-1} with just 5 V applied voltage between plates [61]. The intrinsic traceability of Rydberg atomic sensors also helps establish the calibration of voltage measurement instrumentation. The DC and 60 Hz AC voltages are measured via a cylindrical vapor cell with stainless-steel parallel rectangular plates which are about 2 mm apart from each other. The measurement uncertainty is less than 1.2% [62]. Based on another novel electrode structure which consists of a series of conducting-Si rings, DC electric fields of up to 5 kV m^{-1} were measured [63].

3. Autler-Townes-splitting approach

3.1. Principle

When measuring microwaves using traditional antennas, as the microwave frequency changes, different antennas need to be replaced to maintain a consistent gain. As mentioned earlier, the size of the antenna gradually increases as the frequency decreases. One major advantage of microwave sensors based on Rydberg atoms is that the Alkali-metal atoms possess a highly rich energy level structure, and transitions between neighboring or closely spaced Rydberg states cover the entire microwave frequency range from 300 MHz–300 GHz, reaching orders of terahertz. Therefore instead of changing any hardware, Rydberg atomic sensors only need to vary the frequencies of the excitation laser and adjust the optical power to maintain the sensitivities.

Due to the small overlap of the wavefunctions between ground and Rydberg states, one-step excitation to the Rydberg state requires much higher laser power and the choice for angular momentum is limited to the p state. Normally multi-step excitations to Rydberg states are preferred, which means that in practice, the Rydberg atoms are prepared with a group of lasers. Normally an infrared laser is used to excite atoms from the ground state to the intermediate state, which also serves as probe laser. Other lasers are applied as coupling lasers to drive atoms from the intermediate state to the Rydberg states. Based on these ladder-type energy structures, the coherence between excitation pathways establishes and leads to the phenomenon of EIT in terms of the transmission increase of the probe laser when it is on resonance of the absorption line. the addition of another energy level, coupled with interactions between atoms and microwave field, results in changes in the transmission spectrum of the probing light, leading to Autler-Townes splitting (ATS). By measuring the intensity profile of the optical readout of the probing light, we can directly obtain information about the microwave field's properties including intensities, polarizations, etc. Specifically, the narrow transparent window of the EIT peak would experience ATS, and the frequency gap Δf between two splitting peaks when scanning the coupling laser is

$$\Delta f = \mathscr{P}_{rr'}|E_{EM}|/\hbar, \tag{9}$$

where $\mathscr{P}_{rr'}$ is the transition dipole moment between two adjacent or close Rydberg states which are coupled with EM waves, and E_{EM} is the amplitude of the EM waves. Then the amplitude of the electric component or related intensity of EM waves could be measured through $E_{EM} = \hbar\Delta f/\mathscr{P}_{rr'}$ by measuring the optical frequencies. With this method, the measurement of EM wave intensity is converted into a measurement of optical frequency, which is currently the most precise measurement technique achievable by humans.

3.2. Two-photon-transition scheme

Among various experimental schemes for Rydberg atom excitation, the two-photon excitation process is the most commonly employed. For cesium atoms, the cascaded excitation paths are $6S_{1/2} \rightarrow 6P_{3/2} \rightarrow nS_{1/2}/nD_{3/2,5/2}$ of which the lower transition from ground to intermediate state is driven by the probing laser with wavelength of about 852 nm and the upper transition from intermediate to Rydberg state is realized by coupling laser with wavelength of around 510 nm. For Rubidium atoms, the transitions are $5S_{1/2} \rightarrow 5P_{3/2} \rightarrow nS_{1/2}/nD_{3/2,5/2}$, and the wavelengths of the probe and coupling lasers are 780 and 480 nm, respectively. The

frequencies of either probe or coupling laser should be scanned covering the range of EIT linewidth. If the frequency of the probing light is scanned, the EIT signal will exhibit a significant Doppler broadening background. This is due to the motion of alkali-metal atoms in the atomic vapor cell, which follows a Maxwell-Boltzmann distribution, causing the broadening of absorption lines associated with lower-level transitions. By exploiting the differential detection technique with adding another absorption laser as a reference, the Doppler background would be canceled although the lineshapes of the EIT signals are deformed due to the wavelength mismatch between the coupling and probing lasers. Another method usually applied is scanning the frequency of the coupling laser while locking that of the probe laser to achieve EIT spectrum without the Doppler background [24,64]. The intensities of EM waves could be derived from the ATS spectrum by coupling the Rydberg states with EM waves as mentioned above. The first milestone research work that measured the amplitude of Ku band microwave with frequency around 14.233 GHz was done in the Rubidium vapor cell [65]. At an appropriate microwave intensity, the EIT peak exhibits a distinct ATS spectrum, and the frequency gap between two ATS peaks was linearly dependent on the square root of the microwave power as depicted in Eq. (9). However, as the power of the microwave decreases so that the splitting of the EIT signal is not resolved, the variation of the probe transmission was induced due to the on resonant AC Stark shift caused by a weak microwave electric field. And the minimum detected microwave electric field is 8.33±0.37 $\mu V\,cm^{-1}$, which corresponds to intensity sensitivity of about 30 $\mu V\,cm^{-1}\,Hz^{-1/2}$ considering the integration time of the signal. Furthermore, the polarizations of the microwave are measured under the same scheme, and the angular resolution of 0.5° was achieved [66]. Since then, measurements of microwave electric fields based on the two-photon EIT-ATS phenomenon of Rydberg atoms have captured people's research interest and have seen rapid development in both breadth and depth.

Working bandwidth As mentioned above, one of the unique properties of the Rydberg atomic sensor for the measurement of the electric field of EM waves is ultra-wide frequency band coverage due to the abundant transition frequencies between Rydberg states. The atomic sensor would work in a specific center frequency by tuning the frequency of the coupling laser to a certain Rydberg state. The millimeter wave detection was carried out in the vapor of ^{85}Rb [67]. Microwaves with frequencies of 93.71 and 104.77 GHz which are in the WR-10 band were applied through an open ended rectangular wave guide (OEG) into the atomic vapor cell driving the transitions of $29D_{5/2} \rightarrow 30P_{3/2}$ and $28D_{5/2} \rightarrow 29P_{3/2}$, respectively. The linear dependencies of ATS on the square root of applied microwave power were observed; however, the fluctuations of the measured electric field are within ±20% due to the standing wave effects in the vapor cell. To demonstrate the broadband nature of the atomic sensor, microwaves with frequencies lied in Ku, V and W bands are measured with a single rubidium vapor cell [68]. Then transitions of $nD_{5/2} \rightarrow (n+1)P_{3/2}$ were coupled by microwaves with frequencies of 17.04, 68.64, and 104.77 GHz when n = 50, 32, and 28, respectively. Microwaves with frequencies of 15.59 and 18.65 GHz driving two other transitions of $62S_{1/2} \rightarrow 62P_{3/2}$ and $50D_{5/2} \rightarrow 49F_{7/2}$ were also measured. A vapor cell containing both cesium and rubidium was also used for measuring the microwave electric fields [69]. It not only provides a simple method to measure microwaves with different frequencies at the same time but also demonstrates the non-interacting between two similar species of alkali-metal atoms and assesses the accuracy in the calculation of the relative dipole moments of the various atoms. This mixture of two species of alkali-metal atoms with rubidium and cesium in one atomic vapor cell was also used to record the audio data of two guitars at the same time [70]. Two sets of microwaves with frequencies of 19.623 and 20.644 GHz were amplitude-modulated (AM) with sounds from two distinct guitars. The Rydberg atoms of Rb and Cs received and demodulated the signal to play back the sounds of guitars.

Sensitivity Considering Rydberg atoms as quantum sensors for electric fields, the sensitivity of field strength or microwave power is the most significant figure of merit, and is the "holy grail" to be pursued in the research field. It directly influences the maximum propagation distance R_{max} for detectable microwaves as stated in radar theory [71]

$$R_{max} = \left[\frac{P_t A_e^2 \sigma}{4\pi\lambda^2 S_{min}}\right]^{1/4}, \tag{10}$$

where P_t is radiated power in a particular direction, A_e is the effective area of the receiving antenna, and σ stands for the radar cross section which is a characteristic of the particular target and is a measure of its size as seen by the radar, and λ is the wavelength of detecting microwave, and S_{min} is the minimum detectable signal which is equivalent of sensitivity. It should be noted that for the atomic sensor, σ is approximately the cross-section of lasers along their propagation direction which is also the projection area of atom-light interaction volume perpendicular to the propagation direction of microwaves.

For the precision measurement based on quantum technology, the general sensitivity is strongly dependent on the intrinsic large response of the quantum sensor and decoherence time or effective measuring time, which is in the form of sensitivity $\propto \frac{1}{\gamma\sqrt{T_\chi}}$, where γ is transduction parameter and T_χ is decoherence time that reflects the immunity of the quantum sensor against noise [72]. For the measurement of the electric field of microwaves based on an atomic sensor, the minimum detectable electric field could be expressed in a more explicit way as [37,73]

$$E_{min} = \frac{h}{\mathscr{D}_{rr'}\sqrt{N_{Ry} T T_2}}, \tag{11}$$

where N_{Ry} is the density of uncorrelated Rydberg atoms participating in the measurement, T is measuring time, and T_2 is the characteristic dephasing time of the system. The limit of the sensitivity relying on nonentangled states, i.e., the current scheme of the Rydberg atomic sensor is related to the number of atoms participating in the measurement. The sensitivity is set by the quantum projection noise limit which is the standard quantum limit (SQL) of the atomic sensor [74]. A higher OD with less Doppler width is necessary for sensitivity to reach SQL. However in room-temperature vapor cells, the OD is normally low, and increasing the atomic density and laser intensity would lead to increased dephasing which sets a limit for improvement of sensitivity. Even for the best optimization conditions, the sensitivity in ladder-type EIT-ATS is still approximately 3.5 dB higher than SQL [75].

Even challenging, various work has been done for the improvement of sensitivity of the Rydberg atomic sensor. EIT spectroscopy displaying the absorption features refers to the imaginary part of the susceptibility of the atoms. On the other hand, the real part of susceptibility related to the dispersion properties of the atomic medium could also be detected with changes of the index of refraction which leads to the deflect variation of the probing laser. A prism-shaped vapor cell was applied to measure the deflection of the probing laser, and a minimum electric field of RF waves at 5.047 GHz is 8.25 $\mu V\,cm^{-1}$ corresponding to the sensitivity of ~ 46.5 $\mu V\,cm^{-1}\,Hz^{-1/2}$. When the microwave is detuned to the resonance frequency between the coupled Rydberg states, the separation Δf_δ between ATS is

$$\Delta f_{\delta} = \sqrt{(\delta_{\mathrm{MW}})^2 + (\Delta f_0)^2}, \tag{12}$$

where δ_{MW} is the frequency detuning of microwave, and Δf_0 is separation of ATS with microwave on resonance. The sensitivity was improved by detuning the microwave frequency by greater than a factor of 2 compared to the on-resonant ATS method for measuring microwaves with frequencies of 182 and 208 GHz [76]. Besides ATS separation, the detuning of microwave to the Rydberg states transitions also affected the height ratio of two splitting peaks [77].

Power and frequency fluctuations, i.e., intensity and phase noises of probing laser limit the increase of sensitivity. Compared to the direct detection of a probing laser, an approach of optical interferometer can be used to reduce the noise of the probing laser. Mach-Zehnder interferometer along with a homodyne detection technique was applied to improve the measurement sensitivity to 5 μV cm^{-1} Hz$^{-1/2}$ [78]. For EIT spectroscopy of Rydberg atoms, an obvious conversion between phase and intensity noise exists when the frequencies of probing and coupling lasers are on-resonant with transitions from ground to Rydberg state. Using a Mach-Zehnder interferometer with a homodyne detection method, the oscillations of signal and optical noise versus laser phase could be retrieved, as shown in the following:

$$I = a\cos(\Delta\phi) = a\cos(\Delta\varphi' + \Delta\varphi), \tag{13}$$

where a represents the transmission loss while $\Delta\varphi'$ is the phase shift induced by microwave electric field

$$\begin{cases} a \propto \exp\frac{-2\pi l\Im[\chi(\delta_p,\Omega_{MW})]}{\lambda_p}, \\ \Delta\varphi' \propto \frac{\pi l\Re[\chi(\delta_p,\Omega_{MW}]}{\lambda_p}, \end{cases} \tag{14}$$

where l is the length of the atomic vapor cell, λ_p and δ_p are wavelength and detuning of probing laser, respectively. Ω_{MW} is the Rabi frequency of microwave, and $\chi(\delta_p, \Omega_{\mathrm{MW}})$ is the susceptibility obtained by solving the optical-bloch equations. As shown in Fig. 4, when the frequency of the measured microwave is red-detuned, the maximum signal-to-noise ratio (SNR) can be obtained through phase mismatch between the signal and noise. Specifically, 12 dB enhancement of the sensitivity was achieved at −6 MHz detuned for measuring the microwave at 6.94 GHz [79]. Modulation and demodulation spectroscopy is a commonly used technique for detecting weak signals. For Rydberg atoms electric field sensor, frequency-modulated spectroscopy was applied to improve the SNR of direct optical readout. Sensitivity of ∼3 μV cm^{-1} Hz$^{-1/2}$ is achieved when measuring the microwave with frequency of 5.047 GHz [80]. For amplitude modulation spectroscopy, the intensity of AM was linked with that of microwave. By choosing the detuning of microwave to be −6 MHz, an optimized sensitivity of 12.50(04) nV cm^{-1} Hz$^{-1/2}$ was achieved when AM frequency was 2 kHz [81]. When measuring the electric field that coupled a higher Rydberg transition, the sensitivity was improved to be 5.102(49) nV cm^{-1} Hz$^{-1/2}$ [82]. A scheme of multi-carrier-modulation (MCM) consisting of FM of probing and AM of coupling lasers was applied to increase the SNR by a factor of 2 [83]. Combining the frequency modulation spectroscopy and dispersive detection, 10 times steeper dispersion spectra were obtained and used to characterize the weak microwave electric field as small as 33±6 μV cm^{-1} [84]. Compared to Rydberg atoms in a vapor cell at room temperature, the broadening of EIT spectroscopy due to the Doppler effect would be strongly suppressed in the cold atomic ensemble leading to hundreds of kHz spectral linewidth. The minimum microwave electric field intensity was 430 μV cm^{-1} which is an order higher sensitivity in the EIT-ATS regime than that in vapor cells at room-temperature [85]. On the contrary of EIT, the ATS of electromagnetically induced absorption (EIA) in cold atoms was observed and used to measure the microwave electric field leading to the minimum field strength of ∼100 μV cm^{-1} [86].

Cavity-enhanced spectroscopy could also be applied to the measurement of electric fields based on the Rydberg atomic sensor. The cavity-assisted Rydberg atoms EIT inside an optical cavity had been already realized experimentally [87]. Either the intensity of the microwave or laser could be raised. theoretical proposals had been suggested [88–90], where the transmission spectrum was greatly narrowed due to cavity coupling, and the spectrum resolution was increased by more than 20 times leading to 8 times improvement of the sensitivity than without the cavity [88]. Besides the absorption spectroscopy, intracavity anomalous dispersion was also utilized for weak microwave electric field detec-

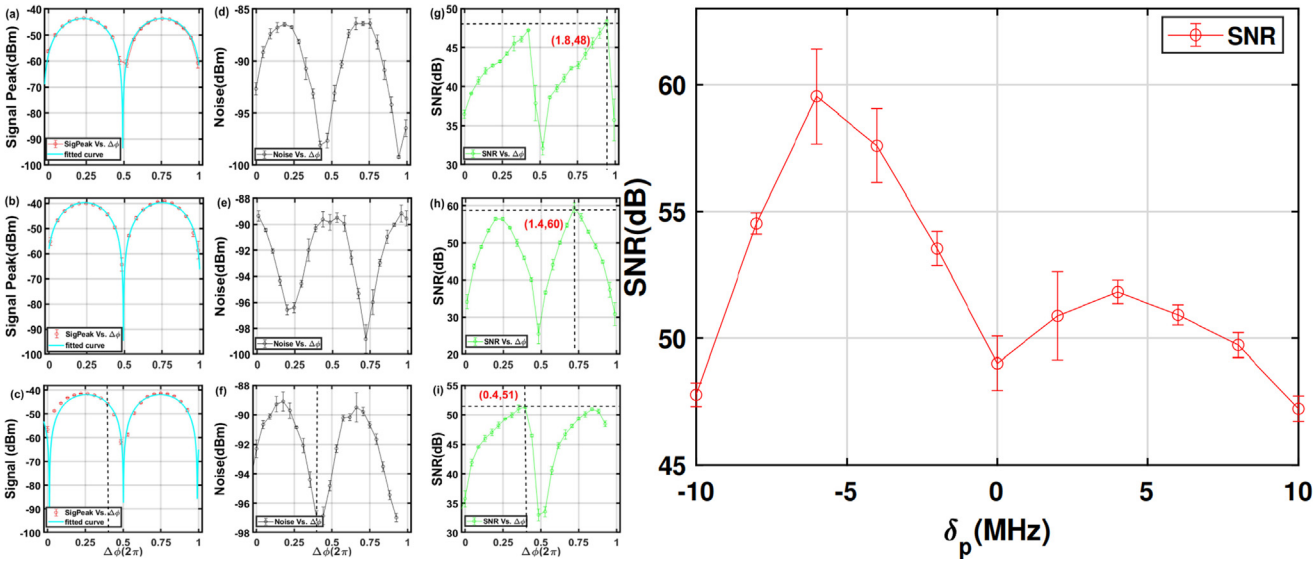

Fig. 4. (Color online) Left panel: Spectrum signal intensities and noise when the Piezo is adjusted. In (a)–(c) the red circles are the peak values of the demodulated signal and the cyan curves are the fitted curves, in (d)–(f) the black circles are the noise, and in (g)–(i) the green lines are the SNR and the coordinates marked in red represent the location and the value of the optimum SNR. For (a), (d), (g), δ_p = 0, for (b), (e), (h), δ_p = −6 MHz, and for (c), (f), (i), δ_p = 6 MHz. Right panel: Output SNR of the MZI as a function of the one-photon detuning δ_p. The results show the SNR is increased by 12 dB when the probe-light frequency is red detuned by 6 MHz from resonance [79].

tion, and 10 times enhanced sensitivity was shown based on numerical simulation than without the cavity [89]. Collective Rabi splitting (CRS) spectrum was proposed to enhance the sensitivity about 7 times higher compared with single atom EIT spectrum [90].

Uncertainty Precision is another inherent feature of the E-field Rydberg atomic sensor. A simple yet traceable chain leading back to fundamental physical constants guarantees a high theoretical measurement accuracy of Rydberg atomic electric field sensor. However, some technical issues should be addressed for uncertainties assessment of the sensor in practical. The linear dependence of ATS on the square root of microwave power as depicted by Eq. (9) is served as calibration for extracting the sensitivity and evaluating the dynamical range of atomic sensor, and the conditions when Ω_{MW} is greater than twice the EIT linewidth ($2\Gamma_{EIT}$) should be satisfied that the linearity of the relation is valid. In this case, the error of the linearity is limited to $< 1\%$ [91]. Compared to the $nS_{1/2} \rightarrow n'P_{3/2}$ and $nD \rightarrow n'P$ transitions, higher degree of linearity on larger scale of microwave strength was maintained for the transitions of $nS_{1/2} \rightarrow n'P_{1/2}$ and $nD \rightarrow n'F$ [92]. If the strength of the microwave decreases, the non-linearity behavior shows, while decreasing the power of both lasers was found to enlarge the linear regime [93]. The vapor cell containing alkali-metal atoms is currently the key element of the atomic sensor. Compared to the conventional metal antenna, the disturbance to the target electric field due to reflection and absorption would be very small by choosing suitable materials. However, the Fabry-Perot (FP) effect causing the standing wave inside the cell would lead to the variation of the E-field of the microwave which introduced the uncertainty for precise field strength measurements. A parameter based on the diffraction of the microwave was suggested to characterize this uncertainty as D/λ_{MW}, where D is the distance between the inner walls of the vapor cell along the propagation direction of the microwave, and λ_{MW} is the wavelength of the microwave. It is found that for the cubic vapor cell made of Pyrex, the variation of the electric field is smaller than $\pm 7\%$ when $D/\lambda_{MW} < 0.08$, which leads to the ± 3 dB uncertainties in the magnitude of electric field [94]. Reducing the thickness of the cell wall also increased the stability of the measured electric field inside the cell, and the restricted wall thickness results in a measurement error smaller than 3% at the center of a vapor cell [95]. The polarization changes of both lasers and microwave when passing through the vapor cell also affected the precision of measurement results, yet it could be compensated by active control of the polarizations of lasers to maintain the optimal relative angle of polarization212s between microwave and lasers [96]. Besides vapor cells, there are some other sources that introduce the uncertainties as fluctuations of frequencies and powers of lasers, the calculation accuracy of transition dipole moment $\mathscr{P}_{rr'}$, and repeatability of the data acquisition processes [97]. The robustness of EIT-ATS spectroscopy against noise was analyzed by measuring the electric field of microwaves in the presence of band-limited white Gaussian noise (BLWGN). The amount of deviation of the EIT-ATS signal under BLWGN is strongly connected to the noise parameters [98].

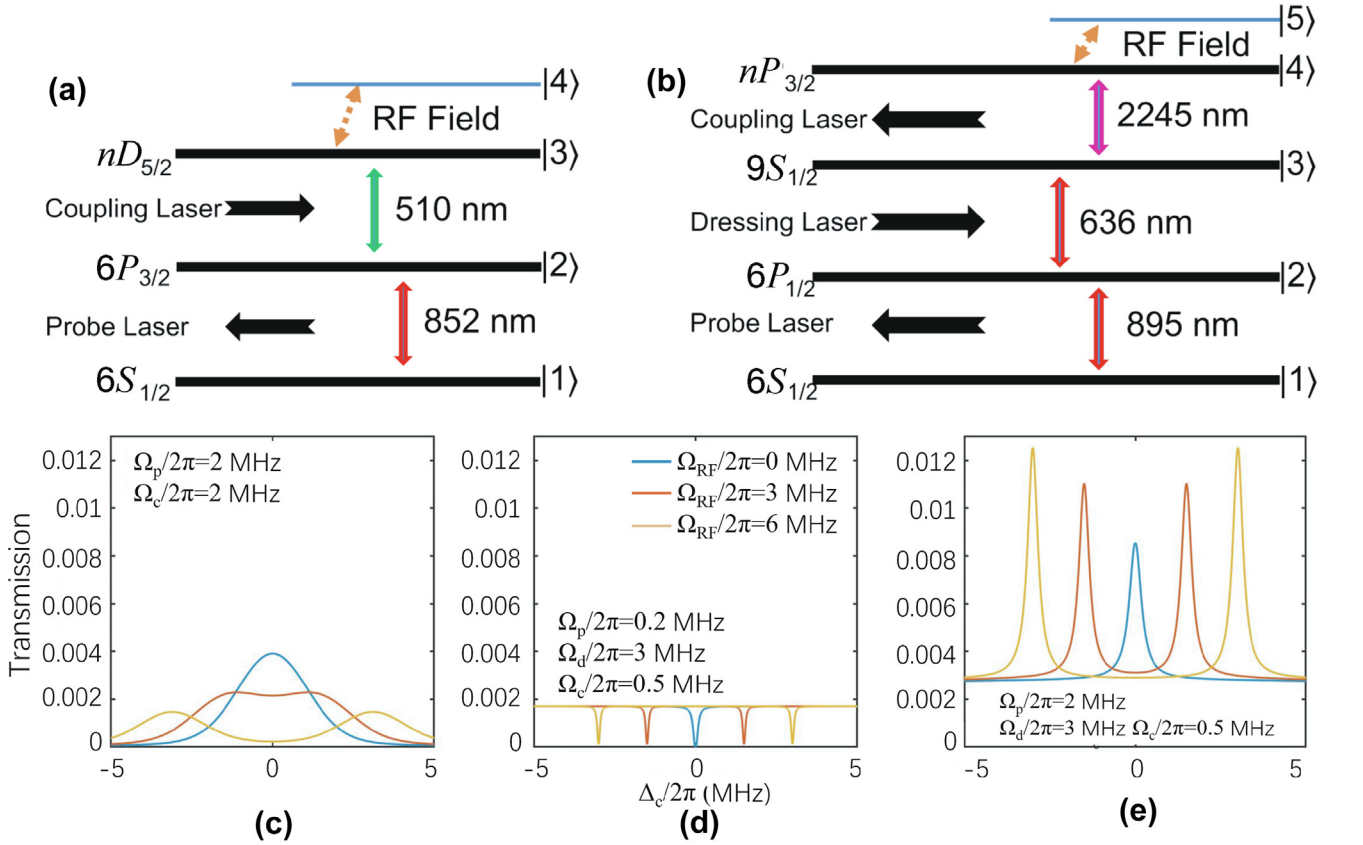

Fig. 5. (Color online) Atomic structure and related interacting lights and microwave of two and three photons excitation and comparison of two-photon and three-photon EIT spectra in ^{133}Cs atoms for laser Rabi frequencies as labeled. The different traces are for different strength radio frequency fields, which is adopted from Ref. [64] (a) Two-photon excitation scheme; (b) three-photon excitation scheme. (c) Two-photon EIT spectrum in ^{133}Cs for different applied RF Rabi frequencies. (d) Three-photon EIA signal resulting from using a probe field Rabi frequency smaller than three-fifths of the coupling Rabi frequency. (e) Three-photon EIT signal resulting from using a probe field Rabi frequency larger than three-fifths of the coupling Rabi frequency. The legend is shared for (c)–(e).

3.3. Three-photon-transition scheme

In the two-photon schemes for excitations of Rydberg atoms, the ability to distinguish ATS is limited mainly by the residual width of the Doppler effect which is about $2\pi \times 3.5$ MHz in cesium at room temperature atomic vapor cell, and through homodyne optical read-out method, the smallest splitting was about $2\pi \times 1.7$ MHz [78]. By utilizing specific col-linear three-photon excitation scheme, the residual Doppler broadening could be greatly reduced [64,99–101]. As shown in Fig. 5, two schemes of two- and three-photon transition energies structures and EIT linewidths comparisons are presented. In the col-linear configuration of three-photon Rydberg state excitation, cesium atoms are excited via $6S_{1/2} \rightarrow 6P_{1/2} \rightarrow 9S_{1/2} \rightarrow nP_{3/2}$ with 895 nm, 636 nm, and 2.245 μm the wavelengths of probe, dressing and coupling lasers, respectively. The linewidth of the EIT peak in three-photon scheme was reduced to $\sim 2\pi \times 39$ kHz compared to that in two-photon scheme of $\sim 2\pi \times 3.5$ MHz [64]. The Rabi frequencies of probe and coupling lasers in Fig. 5c are $2\pi \times 2$ MHz and $2\pi \times 3$ MHz respectively. For three-photon EIA situation as shown in Fig. 5d, the Rabi frequencies of probe, dressing and coupling lasers are $2\pi \times 0.2$ MHz, $2\pi \times 3$ MHz and $2\pi \times 0.5$ MHz, respectively. And for three-photon EIT condition, the Rabi frequencies of probe, dressing and coupling lasers are $2\pi \times 2$ MHz, $2\pi \times 3$ MHz and $2\pi \times 0.5$ MHz, respectively. By coupling $42P_{3/2}$ with $41D_{5/2}$ Rydberg states with microwave at 10.7 GHz, the smallest resolvable ATS is $2\pi \times 503 \pm 6$ kHz which corresponds to an electric field strength of 282 ± 4 μV cm^{-1} [102]. The result is one order of magnitude better than in two-photon excitation configuration. Furthermore, single-photon energy is low of longer wavelengths used for excitation of Rydberg atoms, thus avoiding the ionization shielding effect of alkali atoms in the atomic vapor cell due to photoelectric ionization, which is preferable in low-frequency RF waves measurement [103].

4. Multi-microwave configurations

4.1. Superheterodyne methods

For the method of EIT-ATS approach, it is the resonant transition between neighbouring or nearby Rydberg states driven by microwave field that consists of the scheme of the electric field sensing. The minimum detectable electric field strength of the microwave signal is limited by the linewidth $\Gamma_{\rm EIT}$ of the EIT signal. In thermal atomic vapor cells, the linewidth of the EIT signal is broadened due to various mechanisms, such as power and collisional broadening. One of the most significant causes is Doppler effect according to the velocity distribution of atoms inside the cell. Even though the residual Doppler broadening can be largely suppressed with three-photon-excitation scheme, the intrinsic linewidth of the Rydberg state which is of the order of hundreds of kHz sets the limitation.

Inspired by conventional radio receivers, an atomic superheterodyne receiver for microwave sensing was introduced [104,105], and became a second milestone of development of the Rydberg atomic sensor as the sensitivities are significantly enhanced and the sensor is capable of measuring phases of waves which filled the final gap in achieving full-parameter microwave measurement based on Rydberg atoms. The typical experimental setups are shown in Fig. 6. Besides the signal wave, a relatively strong local field is mixed with signal either through power spilling and both waves are transmitted with one antenna [105] or in the cell and two fields are transmitted separately with two antennas [106].

Sensitivity One of the most noticeable work was done by Jia's group [105], the weak signal wave was mixed with a strong local oscillation (LO) at the frequency of 6.94 GHz, and the beat signal at intermediate frequency (IF) (150 kHz in the experiment) which carries the information of signal field could be demodulated and amplified with Rydberg atoms. In practical, the local microwave induces an EIT-ATS spectrum, and the minimum of probe laser transmission is located at the position where the slope of each EIT line is $|\kappa|$ which holds the maximum magnitude when the separation of ATS equals the linewidth of single EIT peak.

The change of the optical power is

$$P_{\rm out}(t) = |P(\delta_s)| \cos(2\pi\delta_s t + \phi_s), \tag{15}$$

where δ_s and ϕ_s are frequency detuning and phase differences between signal and LO wave. $|P(\delta_s)|$ is the amplitude of the single-sided Fourier spectrum of $P(t)$ at linear frequency δ_s. The Rabi frequency Ω_s of the signal is measured as

$$\Omega_s = \frac{|P(\delta_s)|}{|\kappa_0|}, \tag{16}$$

where $|\kappa_0|$ is the optimal slope. Then the signal amplitude was derived as $E_s = \left(1/\sqrt{2}\right)\hbar\Omega_s/\mu$. Both $|\kappa_0|$ and $|P(\delta_s)|$ could be directly obtained from the optical spectrum.

As mentioned above, the linear dependence of ATS on the square root of microwave power is valid when the power is in the mediate range where the splitting is clearly resolved. As the power of microwave decreases, the non-linearity behavior dominates, that is when $\Omega_s < \Gamma_{\rm EIT}$, the sensitivity $S \propto \sqrt{\sigma}$ where σ is a classical noise-induced error. The minimum detectable electric field is $E_{\rm min} = S/\sqrt[4]{T}$. For atomic superhet detection, the linearity continued even though $\Omega_s \ll \Gamma_{\rm EIT}$, then the preferred $S \propto \sigma$ and $E_{\rm min} = S/\sqrt{T}$ are valid of which the sensitivity reached 55 nV cm^{-1} Hz$^{-1/2}$ as shown in Fig. 7. By reducing the technical noise affecting the long-term stability of the system, within 1% random fluctuation the measuring time lasted 5000 s, which gave the minimum detectable electric field strength of 780 pV cm^{-1}. However, the linearity broke down when $\Omega_s \sim \Omega_L$, and for $\Omega_s > \Gamma_{\rm EIT}$, a linear detection of E_s is reliable via EIT-ATS measurement. Similar results were obtained when measuring the signal wave at 19.62609 GHz mixed with a strong local wave at 19.626 GHz, which gave the IF signal at 90 kHz. The minimum detectable electric field strength is about $\approx 460 \pm 20$ nV cm^{-1} which corresponds to the sensitivity of 790 nV cm^{-1} Hz$^{-1/2}$ [104]. Later, the sensitivity was further improved by introducing a repumping laser for adjusting the ground state atomic population [107]. The EIT amplitude was doubled without the width increase of the peak, indicating that the maximum slope at the half width of the EIT spectrum was also doubled leading to $\approx$ 30 nV cm^{-1} Hz$^{-1/2}$. Combining atomic superheterodyne and three-photon EIA phenomenon leads to the sensitivity of 55.79(23) nV cm^{-1} Hz$^{-1/2}$ when measuring the microwave at 1.18988 GHz [108].

Apart from the detection scheme based on the resonant or near-resonant coupling of adjacent Rydberg states by microwave, the application of local strong field is also an effective method to improve the sensitivity for measuring RF signal at low frequency regime based on off-resonant Stark effect [103,109,110]. In the work described in Ref. [103], there is a 30.05 MHz LO field and a 30 MHz signal field with $\phi_{\rm LO} = \phi_{\rm sig}$ the vapor cell, resulting in a beat note spectrum as shown in Fig. 8, which can be explained by the form of the time averaging frequency shift $\bar{\delta}$:

$$\bar{\delta} = \bar{\delta_0} - \frac{1}{2}\alpha E_{\rm LO} E_{\rm sig} \cos\Delta\omega t. \tag{17}$$

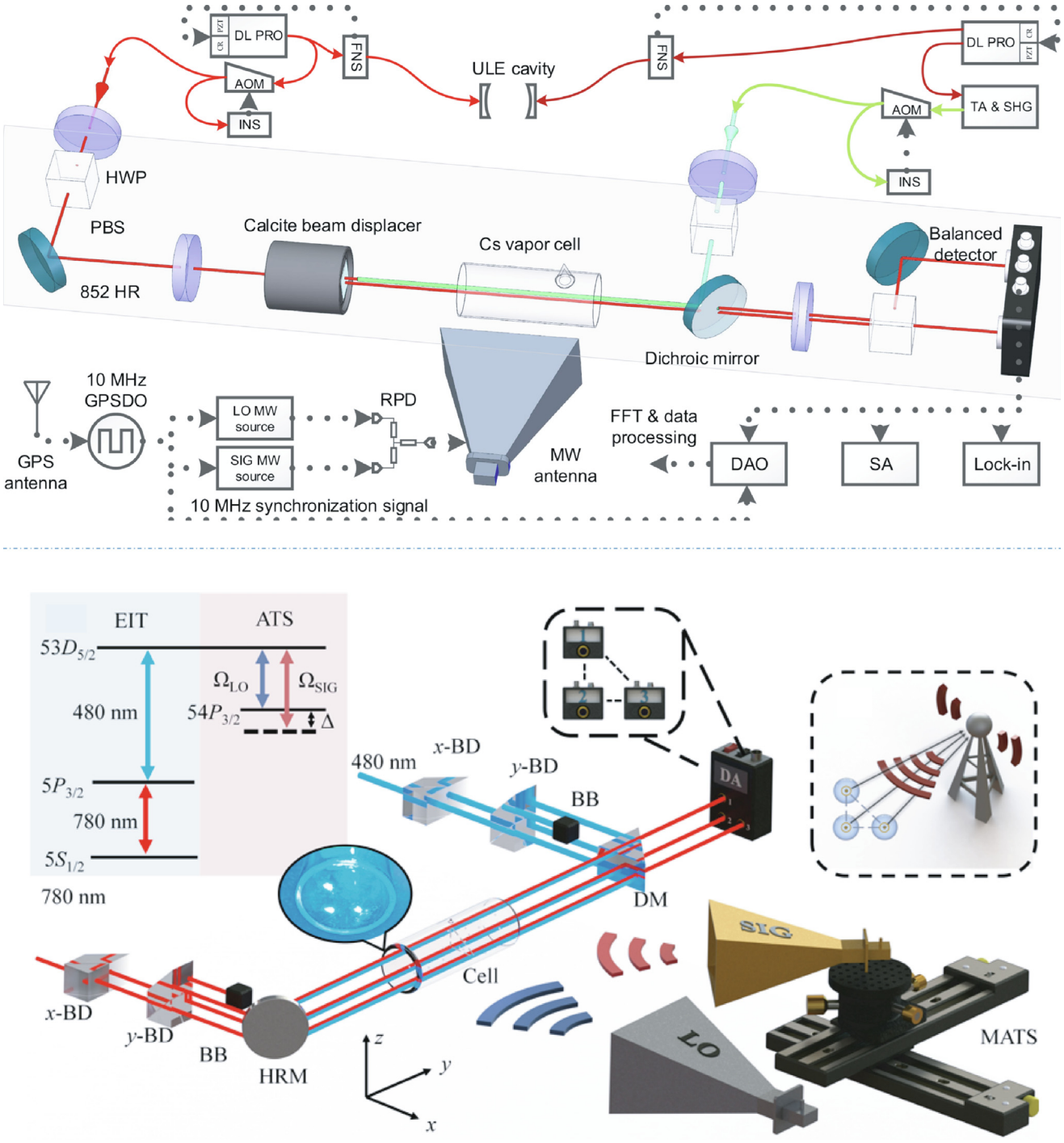

Fig. 6. (Color online) Typical setups of an atomic superheterodyne microwave sensor. The local and signal waves are mixed and transmitted with one antenna as shown in upper panel [105], or two antennas, separately depicted in lower panel [106].

By varying the power of LO field (P_{LO}) and the detuning of LO field and signal field ($\Delta\omega$), a minimum E field strength of 37.3 μV cm^{-1} Hz$^{-1/2}$ and a 3-dB instantaneous bandwidth of 0.8 MHz are derived.

To get the information of the magnitude of the signal frequency, the beat-frequency components of the probe light are analyzed and extracted. As shown in Fig. 9, the data dots extracted from the system fit the original sinusoidal and square-wave functions well with a fidelity of 98%. With the frequencies of the LO field and signal wave scanned continuously, the universal sensitivities of 712 nV cm^{-1} Hz$^{-1/2}$ were realized with dynamical range of over 65 dB [109] (see Fig. 10).

As described in Eq. (11), the minimum detectable electric field is related to the inverse of the square root of atomic number, and the relationship between the atomic superheterodyne receiver's sensitivity and the number of atoms involved in the measurement was investigated [111], and the results show that for the ideal case where only interaction noise is present and the RF waves are uni-

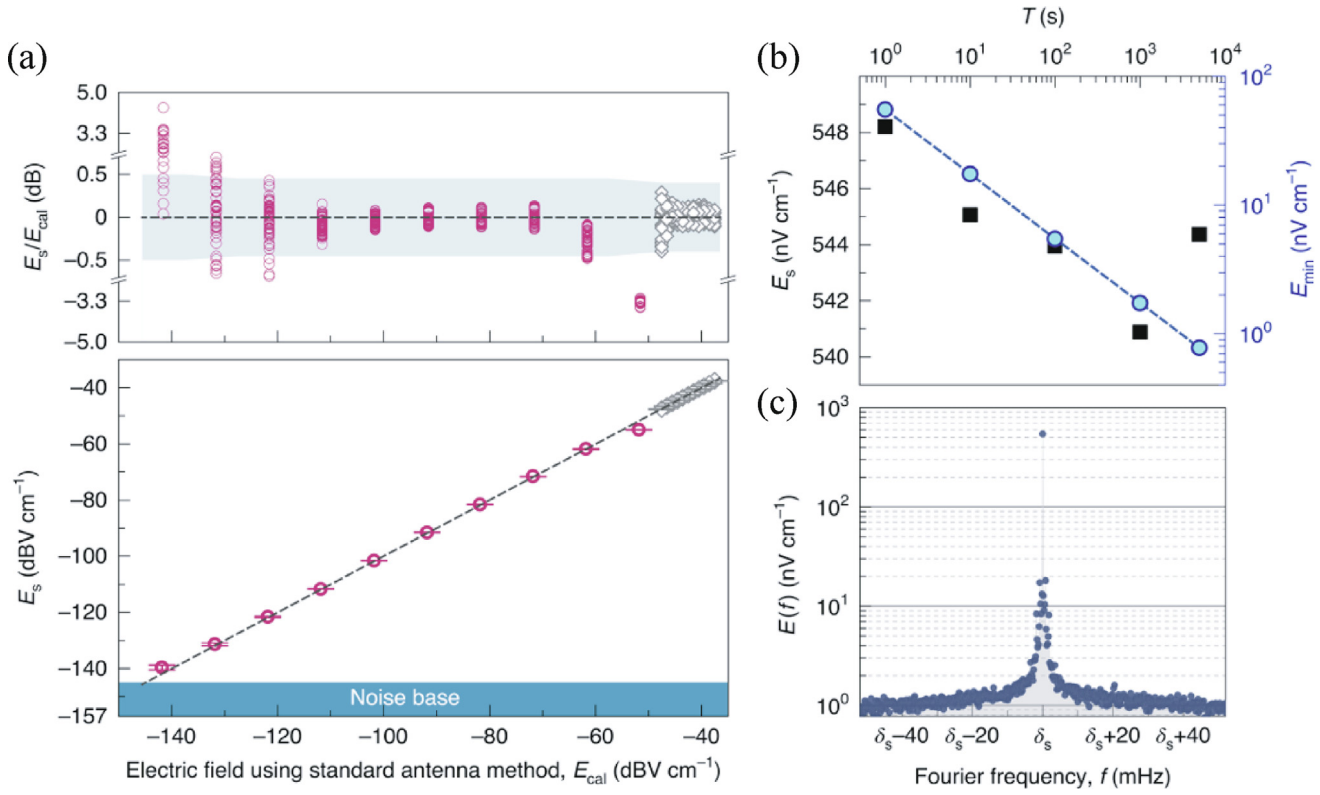

Fig. 7. (Color online) Sensitivity and uncertainties of the electric field measurement based on atomic superheterodyne scheme [105]. (a) Electric field E_s, measured by the atomic superhet, compared with electric field E_{cal} measured by the standard antenna method. (b) Measurements of the same MW signal by the atomic superhet at different measurement times T. (c) A single-sided Fourier spectrum of MW field $E(f) = \left[\hbar/\left(\sqrt{2}\mu\right)\right]|P(f)|/|\kappa_0|$ measured at T = 5000 s. From the peak we derive an SNR of 57 dB, agreeing with the SNR predicted from the preset electric field value via the standard antenna method. In all panels, δ_s=150 kHz. See Ref. [105] for details.

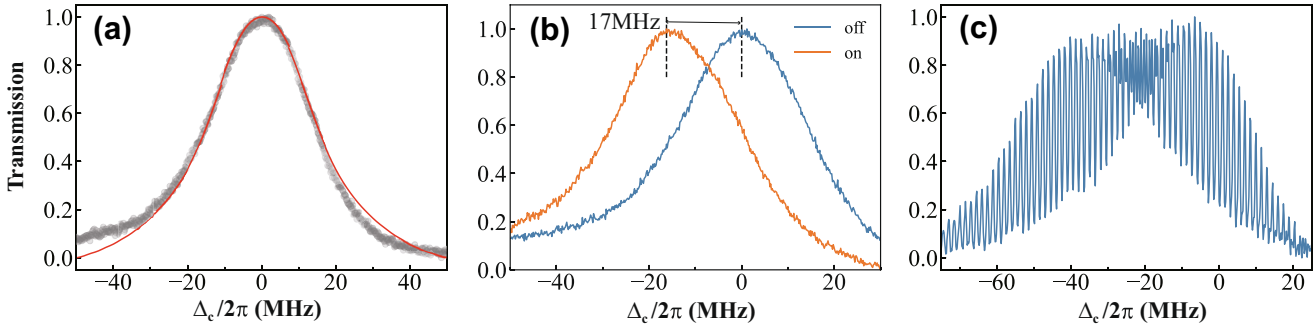

Fig. 8. (Color online) (a) Three-photon EIT spectrum of Cs atoms. The gray dots are the experimental data, and the red line is the theoretical result. (b) EIT spectrum in an external RF electric field. The RF electric field causes the EIT spectrum to shift to the left. The blue is the spectrum when the RF electric field is turned off, and the orange corresponds to the spectrum when the RF electric field is turned on and P = 8 dBm. (c) EIT spectrum of the Cs atoms when two electric fields are applied, where f_{sig} = 30 MHz and f_{LO} = 30.05 MHz. The EIT spectrum is modulated with $\Delta\omega$ = 50 kHz by the beat signals of the two electric fields. The transmission in the pictures is normalized [103].

formly distributed, the sensitivity of the atomic superheterodyne receiver exhibits a quantum scaling: the amplitude of its output signal is proportional to the atom number which is varied simply by changing the interaction length determined by the laser path, and the amplitude of its read-out noise is proportional to the square root of the atom number. Hence, its sensitivity is inversely proportional to the square root of the atom number. To achieve the near SQL sensitivity, besides the optimization of SNR, the noise analysis of the atomic superheterodyne microwave receiver also affected the ultimate sensitivity. To avoid the non-uniformity distribution of laser power in its cross-section, Wang et al. [112] decorated the laser from Gaussian distribution to flat-top profile. The number of atoms is precisely controlled by changing the diameters of flat-top excitation laser beams. It was shown that under the experimental conditions that the diameters of excitation beams are less than or equal to 2 mm and the read-out frequency is larger than 70 kHz, the sensitivity of the atomic receiver is limited only by the quantum noise and, in the other conditions, limited by classical noise.

Phase measurement Another prominent feature of the atomic superheterodyne method is its intrinsic ability to measure phases of microwaves [105,113]. The Rydberg atoms are mixer to convert the microwave several GHz to an IF signal in the kHz regime. The phase of the IF is directly linked to the relative phase between the local and signal microwave, and since the phase of local field is known and well controlled, then the phase of signal would be obtained.

Based on the Rydberg atom superheterodyne phase measurement method, the angle of arrival (AOA) of an RF signal in two [114] and three [106] dimensional space was demonstrated. By

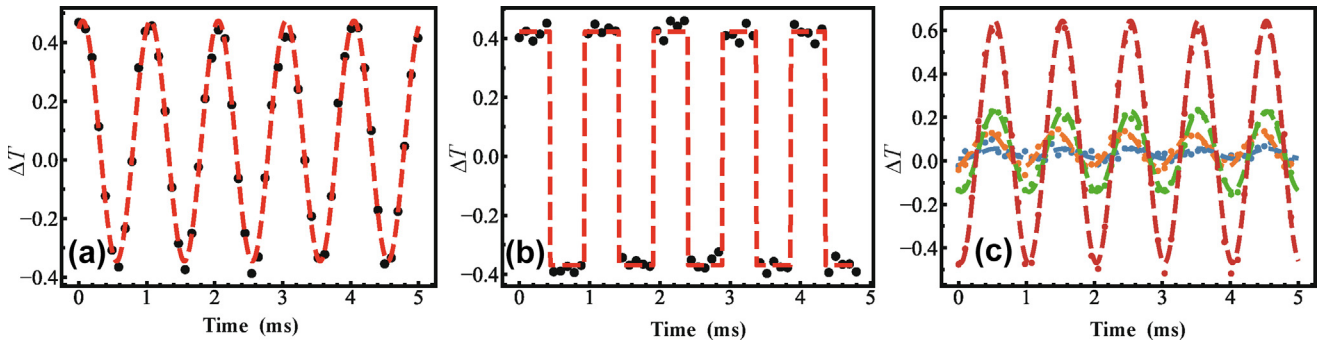

Fig. 9. (Color online) Results of demodulation of a 30-MHz carrier wave. (a), (b) Signals obtained by demodulating the carrier with sinusoidal modulation and square-wave modulation, respectively, with a modulation frequency of 1 kHz. The signal is well restored with 98% fidelity for both sinusoidal and square-wave modulations. The black dots represent the signal after demodulation using Rydberg atoms, and the red dashed line is the modulated signal. (c) Signals obtained by Rydberg atomic demodulation at different modulation depths, 2% (blue), 5% (green), 10% (orange), 30% (red) [103].

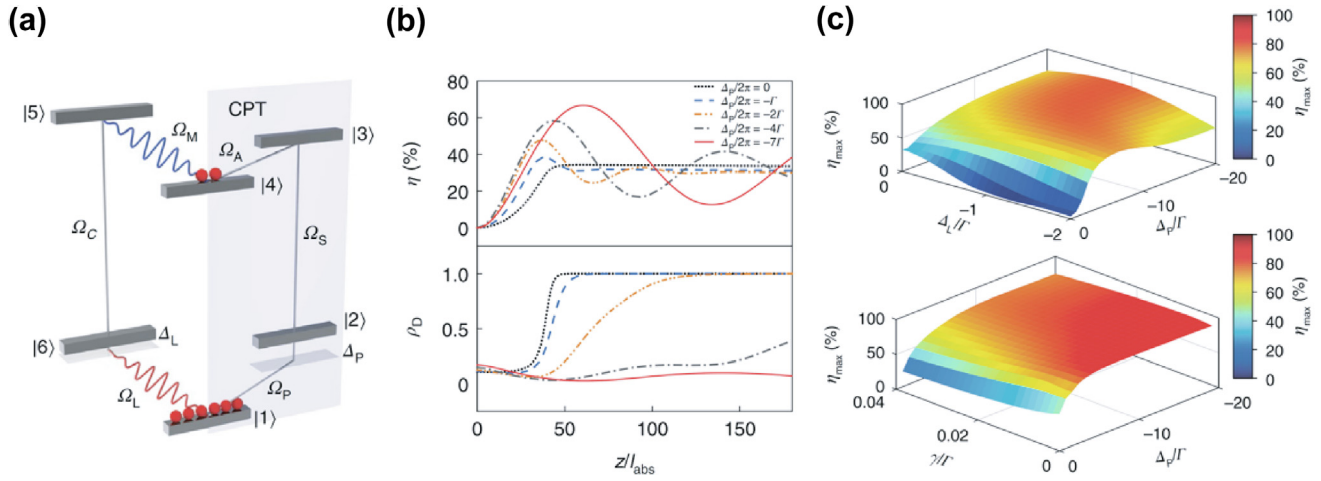

Fig. 10. (Color online) Microwave-to-optics conversion via off-resonant six-wave mixing. (a) Atomic energy-level configuration. (b) Conversion efficiency versus the propagation distance z for different probe laser detunings. (c) Maximum efficiency as a function of the detunings and the Rydberg dephasing rate [119].

measuring the phase difference between the local and signal fields with specific geometry relations, an angle resolution of 1° was achieved in the 2-D situation. The concluded validity of 3-D configuration in the testing scene remains at approximately 90% with a theoretical maximum location tolerance of 5.7 mm.

Apart from applying a local microwave in the atomic superheterodyne configuration, a full optical interferometer within internal-state of Rydberg atoms was suggested [115]. They have constructed the interferometric loops in the state space $(6P_{3/2}, 90S_{1/2}, 91S_{1/2}, 90P_{3/2})$ of cesium and employed them to measure phase and intensity of a 5 GHz microwave in a room-temperature vapor cell. Electromagnetically induced transparency on the $6S_{1/2} \rightarrow 6P_{3/2}$ transition serves as an all-optical interferometer probe. The microwave phase is measured over a range of π, and a phase resolution of 2 mrad is achieved.

Bandwidth The working bandwidth of Rydberg sensor for microwave extends from Hz to THz regime according to the abundant energies structure of Rydberg atoms as mentioned above. The versatility of single atomic antenna covering the ultra-wide frequencies scaling provides convenience for applications requiring receiving signals with varied center frequencies. However, the instantaneous bandwidth which reflects the abilities of the atomic antenna to handle the varied frequency recognition instantly is more practical. The atoms in room-temperature atomic vapor cells move very fast leading to short interaction time with lasers and microwaves as the small beam size in most of the experiments, and hence the limited transit time set an intrinsic barrier for obtaining a higher instantaneous bandwidth. In the configuration of the superheterodyne Rydberg antenna structure, the strength of the IF signal decreased fast within a limited bandwidth, which is normally hundreds of kHz. One effective way to increase the instantaneous bandwidth while holding high sensitivity is to increase the interaction area between Rydberg atoms and lasers and microwaves. While expanding the laser beam would decrease the Rabi frequency of the lasers, then multi-beam scheme is chosen. The instantaneous bandwidth is increased to 6.8 MHz with a reasonable sensitivity. Recently, physical mechanism of six-wave mixing was introduced to assign the intermediate frequency which is frequency difference between local and signal microwave to be the positive and negative sidebands of probing laser, and an instantaneous bandwidth of 10.2 MHz with sensitivity of 62 nV cm^{-1} Hz$^{-1/2}$ was achieved [116].

4.2. Auxiliary microwave methods

In addition to the local strong field used in atomic superheterodyne detection of microwave field, microwaves coupling more Rydberg transitions would help to enhance the ability of the Rydberg atomic microwave sensor.

Compared to the atomic superheterodyne scheme in which the local and signal field coupled the same Rydberg transition, an auxiliary microwave coupling adjacent Rydberg transition greatly

extended the bandwidth response of the atomic sensor [117]. Liu et al. [118] showed that with two off-resonant microwaves working as a tunable local field, the heterodyne receiver can retrieve the amplitude, phase, and frequency information of signal microwave in a continuous frequency band. Sensitivity of up to 1.5 $\mu V\,cm^{-1}\,Hz^{-1/2}$, and continuous frequency range of 1 GHz have been realized. Combining atomic superheterodyne and auxiliary microwave field interactions, the atomic sensor works efficiently for detecting microwave fields detuned by up to 100 MHz with sensitivity increased by a factor of 10 compared to without applying the auxiliary dressing field [39].

5. Microwave-to-optical conversion

With the rapid progress in quantum computing, various platforms have been proposed to up-convert the radiation of microwaves into that of the optical domain, which offers the prospects of the quantum optical interface and quantum networking. Besides the long-term vision, the low-noise microwave detection would benefit from the photon upconversion into the optical domain owing to its well-developed single-photon detector and low thermal occupancy in ambient environment. With the assistance of the driving fields, the Rydberg ensemble serves as an atomic transducer to absorb microwave photons and generate optical light.

Early experimental demonstrations had been carried out in cold atoms. The first effort came from the Li's group [119] at NUS that followed a scheme based on all-resonant fields, and the conversion from ≈80 GHz microwave to ≈780 nm light was realized in a cloud of dilute ^{87}Rb gas. However, the population of atoms would be gradually trapped in an undesired dark state, which was decoupled to the relevant fields in the wave-mixing process. They showed a conversion efficiency of ∼ 5% and a bandwidth of 4 MHz [119]. To boost the conversion efficiency, the Yan's group [120] of SCNU proposed that the off-resonant coupling prevented the build-up of population in the dark state, as shown in Fig. 5. Their experimental system employed a two-dimensional magneto-optical trap that provided a high OD and a low Rydberg dephasing [120], and realized an efficiency of up to 82% over a large range of microwave intensity with mean photon numbers ranging from 50 to 6400.

In the free-space upconversion, the interaction area is defined by the auxiliary laser beams, while the microwave radiation is unable to be focused into such typically sub-wavelength volume. In order to quantify the overall conversion efficiency, the whole power of the incoming microwave should be considered, for instance, in an implementation where the single-mode microwave is confined by a waveguide and an elongated atomic converter is placed in the waveguide core. Interestingly, Ref. [121] concluded that the subwavelength transverse area can be compensated with the longitudinal extension of interaction volume in the waveguide. Consequently, the confinement mode still enabled high efficiencies close to the theoretical limit in the free-space setting, as long as the atomic ensemble possesses a sufficiently large OD that is required to complete the conversion. Recently, Kumar and colleagues [122] coupled a cold atomic ensemble simultaneously to a superconducting resonator and optical cavity, and demonstrated a microwave-to-optical conversion with an overall efficiency of 2.5% in the four-wave mixing process.

The cold Rydberg converters are bound to operate in the impulse regime due to the magneto-optical trap preparation sequences, and typically exhibit a bandwidth of a few megahertz. A more recent experiment proposed by Borówka et al. [123] extended the microwave upconversion to the continuous-wave regime by the use of room-temperature vapor cells. In the all-optical scheme, the converter demonstrates a wide bandwidth of 16 MHz and a dynamic range of 57 dB, from the saturation limit descending down to the thermal noise level (2.1×10^3 photons per second). Unlike the previous free-space conversion, the single-photon counter is used instead of the photodetectors with high background noise. The converter's non-thermal noise corresponds to a noise-equivalent temperature T_{NE} = 53 K. Remarkably, after adding the cavity-assisted filtration of the thermal signal, the signal-to-noise ratio is improved and thus T_{NE} is descending down to 3.8 K, demonstrating the sensitive photon-based MW detection. They concluded that the advantages of warm-atomic conversion, such as the modest setup, adaptability, and low noise figures, reveal its potential applicability in areas such as radio astronomy.

6. Non-equilibrium state sensing

Unlike uncorrelated atoms in room-temperature vapor cells, interacting many-body systems display enhanced sensitivity. Many-body critical enhanced metrology for sensing of external microwave field in non-equilibrium Rydberg atoms was realized [124]. As shown in Fig. 11, due to the interaction, the spectrum shows a population-dependent frequency shift $V\rho_{rr}$ leading to a steep edge of ρ_{rr}

$$\frac{d\rho_{rr}}{d\Delta}|_{\Delta=\Delta_c}=\frac{1}{V+\sqrt{\left(\Gamma^2+2\Omega^2\right)/3\rho_{rr}^2}}, \tag{18}$$

the enhanced sensitivity originates from the increase of derivative of ρ_{rr} and can be expressed in terms of fisher information (FI) as

$$F(\Delta)=\frac{\bar{\mu}'(\Delta)^2}{\mathrm{Var}(\mu)}, \tag{19}$$

where Δ is the parameter to be determined and $\bar{\mu}$ represents the mean value of the difference in photon numbers accumulated in fixed time intervals by a differential detector exposed to a reference beam and a beam passing through the atomic cloud. $\mathrm{Var}(\mu)$ is the variance of the differential signal, that is, the sum of the variances of the two separate and independent counting signals. The sensitivity was estimated to be 49 $nV\,cm^{-1}\,Hz^{-1/2}$.

7. Application overview

7.1. Metrology

It is clear to see from Eq. (9) the simple and essential relation between measured electric field and fundamental physical constant, i.e., the Planck constant. It makes the Rydberg atomic sensor an ideal platform for SI-traceable standards of electric field strengths or voltages, and also a robust tool for antenna calibrations. Due to the simple and robust SI traceable link of the Rydberg atomic electric field sensor, the field distribution of fundamental mode in the waveguide contained a Rydberg atomic vapor cell and then determined the power carried by the wave at both 19.629 and 26.526 GHz from the measured electric field. The comparison between the atomic sensor and conventional power meter was made that showed some discrepancies at higher power level [125]. Characterization of antenna's gain is another fundamental application in the research field of metrology. The quantum-based gain characterization process and results were compared to those featured with conventional three-antenna-extrapolation methods. The Rydberg atoms-based method showed its advantages of simplicity, accuracy, and low cost [126].

7.2. Communication

Another intuitively considered application of atomic microwave sensors is its feasibility in communication fields. High sensitivity

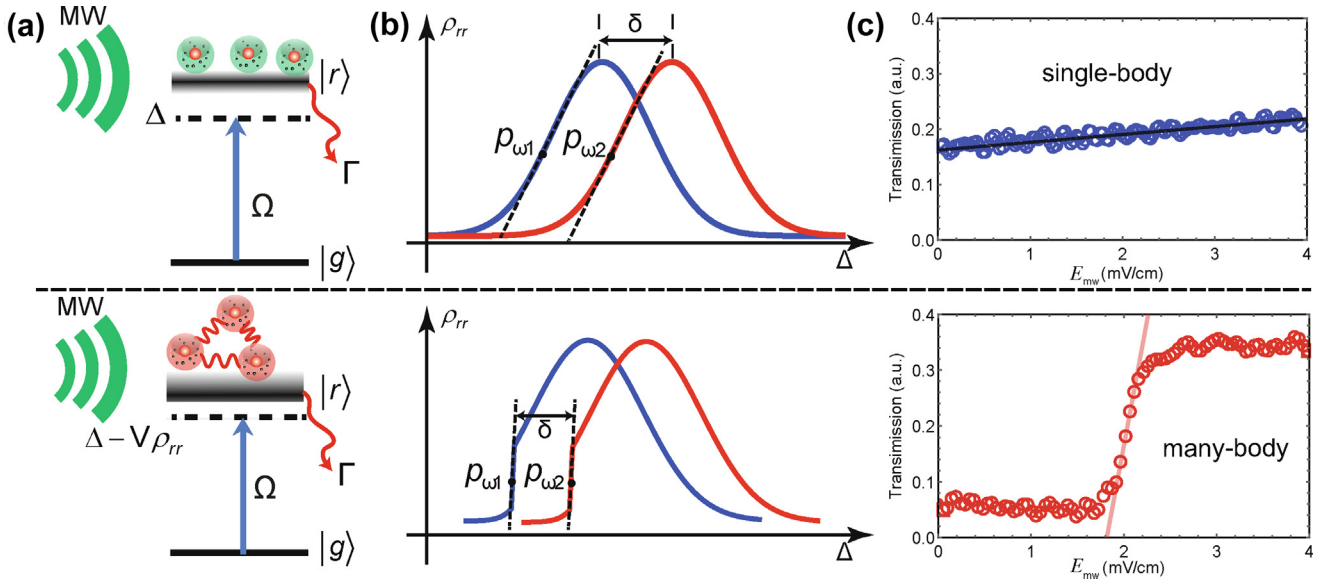

Fig. 11. (Color online) Principles of single-body (top row) and many-body (bottom row) Rydberg metrology. (a) Energy diagram for a two-level atom showing the ground state $|g\rangle$ and Rydberg state $|r\rangle$. In the many-body case, the Rydberg resonance is modified by the many-body interaction strength, $V = C_6/r^6$. (b) The blue and red curves respectively represent the spectrum with and without an external microwave field, which induces a shift δ. The measurement sensitivity is highest when the derivative $d\rho_{rr}/d\Delta$ is maximal, as indicated by points p_{w1} and p_{w2}. The steeper slope near the critical point in the many-body case (bottom row) results in enhanced measurement sensitivity. (c) Transmission under different microwave field amplitudes for the single-body and many-body cases. The steep edge at E_{MW} = 2.0 mV cm^{-1} indicates that the tiny variance of the microwave field induces a giant change in the transmission, and thus the sensitivity of the many-body case is higher than that of the single-body case [124].

together with wide bandwidth leading to larger data capacity according to Shannon theorem are two of the most concerned metrics in the application of communications.

$$C_{SQL} = f_d \log_2\left(1 + \frac{\delta\omega^2 N}{f_d^2}\right), \tag{20}$$

C_{SQL}, as calculated with Eq. (20), is the data capacity limited by the SNR and received bandwidth (f_d). In contrast with its counterpart of classical communication antennas, the quantum antenna based on Rydberg atoms is effective with sensing volume 10^7 smaller than λ^3. The data capacity ranged from 10 kHz to 30 MHz [127]. By encoding the data with amplitude modulation of 17 GHz microwaves, the photon-shot-noise limited channel capacity is measured up to 8.2 Mbit s^{-1} and 8-state phase-shift-keying digital communication protocol was realized [128]. The baseband signal with a carrier frequency of 16.98 GHz was received with fidelity of >95% and baseband bandwidth of about 60 kHz and dynamic range over 30 dB were tested [129]. Using bit-error-rate (BER) as an indicator for the quality of digital communication when demodulating an AM signal, the tunable bandwidth of 200 MHz at a carrier frequency of 10.22 GHz with BER = 0 was realized, and the digital communication at a rate of 500 kbps was performed [130]. As shown in left figure of Fig. 12. Based on the precision measurement of phase of signal microwave and ability to demodulate the PM signal, various digital communication protocols were applied using Rydberg atoms as receivers. Signals decorated with binary phase-shift keying (BPSK), quadrature amplitude modulation (QAM), and quadrature phase-shift keying (QPSK) were received and demodulated to receive data from a phase-modulated communication signal in the configuration with [131] or without local microwave field [132]. AM and FM microwave communication in the baseband around 100 kHz with carrier frequencies in the range of C-band and Q-band were demonstrated [133].

Rydberg atoms are sensitive to both on- and off-resonant microwave radiation as described above. Then built upon the foundation of single-carrier-frequency communication, a multi-frequency, that is frequency-multiplexing scheme can be employed to further facilitate the implementation of more sophisticated communication protocols and carry a greater amount of information. The Rydberg atom-based frequency division multiplexing (FDM) in microwave communication was conducted with the maximum acceptable data transfer rate of both AM and FM about 200 kbps, whereas their maximum BER is less than 5% [134]. Based on Rydberg atom-based heterodyne detection scheme with one local field and three signals with different detunings to local field that consists of a three-channel frequency division multiplexing setup, low BER communication with high symbol rate of 12 kbit/s and weak carriers amplitude of 13 μV cm^{-1} were achieved simultaneously [135]. Multi-receiver channels consist of multi-optical paths that increase the data capacity with BW × $\log_2(1 + N \times \text{SNR})$, where BW and N stand for bandwidth and the number of signal channels [136]. As shown in the right figure of Fig. 12, a more practical example was presented for the investigation of the effect of beam size on the bandwidth for receiving the TV stream. In the experiment, 85 μm beam width is optimal for receiving a live 480i video stream with atomic sensor [137]. By driving the Rydberg atoms to different neighbouring states simultaneously, it demonstrated a digital communication protocol, receiving on–off-keyed binary data from four bands at the same time spanning nearly one decade of frequency [138]. To increase the response speed of Rydberg sensors, an architecture of spatiotemporal multiplexing (STM) of the probe laser was proposed. The bandwidth was demonstrated over 100 MHz, and the feasibility of error-free communications up to 100 Mb/s with an STM Rydberg sensor was predicted with numerical model [139].

The bandwidth within which a communication device can receive signals simultaneously guarantees large data capacity as shown in Eq. (20), hence it is vital for enhancing the ability of

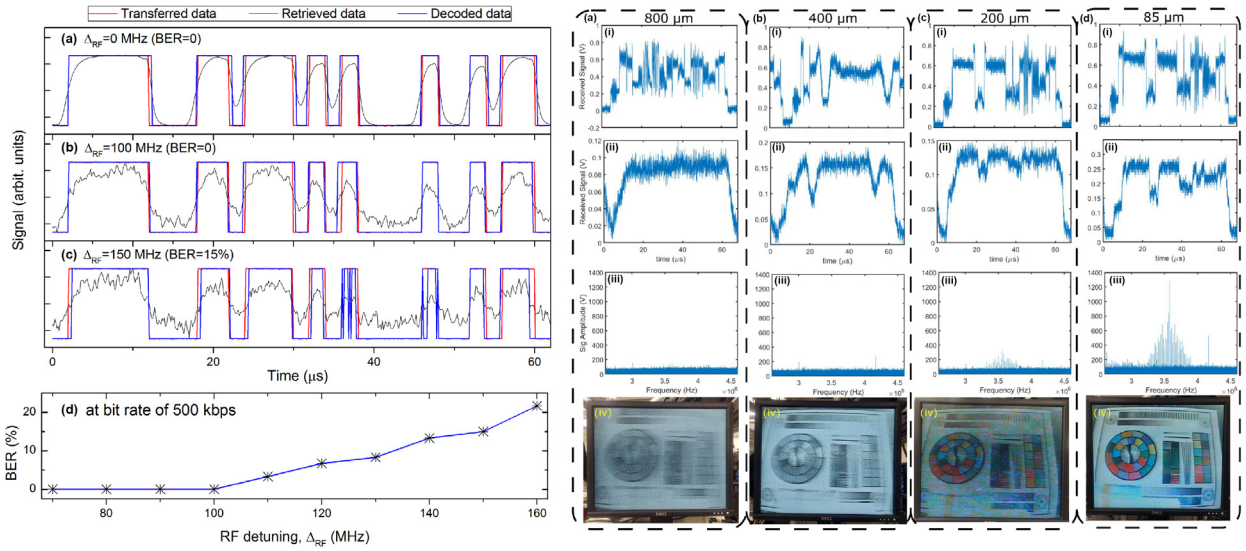

Fig. 12. (Color online) Left: A digital communication tested using a benchmark of PRBS signal transferring at a bit rate of 500 kbps. Three typical waveform transfers are shown in (a), (b) and (c), respectively, corresponding to RF-detuning 0, 100 and 150 MHz with respect to the on-resonant frequency (10.22 GHz). The BER determined by comparing the decoded and source digital signals rises up with RF-detuning, up to 20% at Δ_{RF} =160 MHz in (d) [130]. Right: (a)–(d) Columns show sent and received data from the camera for different beam sizes as labeled. (i) Live video signal from video camera for a given row in NTSC video format. (ii) Signal received by the atoms for the same rows as (i). (iii) The fast Fourier transform (FFT) of the received signal. This is done for two full fields of data acquired. (iv) Video received for the different beam sizes for the given column [137].

atomic sensors as terminals in the communication field. The atomic superheterodyne method greatly raised the level of metrics of sensitivity, while only signals whose frequencies are around the LO frequency in the range of bandwidth can be received with a high SNR. As the frequency of the LO microwave field in the super-heterodyne scheme is fixed at a time. Frequency-comb can be utilized for the purpose of reaching higher instantaneous bandwidth. A frequency comb is a source whose spectrum consists of a series of frequency lines with identical spaces. The history of frequency comb dates back to nearly twenty years ago when optical frequency comb (OFC) was born and has been widely used for atomic clock comparison, atomic clock network, ultra-low-noise microwave generation, etc., for its all harmonically related and phase coherent optical modes [140]. Due to the need to bridge the vast gap from 9.193 GHz cesium frequency to the optical domain, a new optical frequency metrology scheme was designed, which was capable of measuring frequencies across the visible and near-infrared spectrum, with a 300 THz fs laser comb [141]. However, microwave frequency combs have not been applied in RF microwave metrology since then for a long time.

In recent years, Zhang et al. [142] exploited two microwave frequency combs (MFC) to conduct measurement for aiming RF signal. In the spectrometer, a five-level lambda system is used to pump Rubidium atoms to the Rydberg state, as shown in Fig. 13. Instead of providing a single-tone LO microwave field to get the beat signal, atoms are immersed in an MFC consisting of a series of peaks with a fixed repeating rate f_r in the frequency realm. On this occasion, the total field is written as

$$E_{\text{atom}} = \sqrt{N_L} \mid E_{\text{LO}} \mid + \frac{1}{\sqrt{N_L}} \mid E_s \mid \cos \Delta\omega_k t + \Delta\phi_k, \tag{21}$$

where N_L represents the number of MFC peaks, E_{LO} represents the common value of all the MFC peaks, E_s represents the signal amplitude with $E_s \ll E_{\text{LO}}$, $\Delta\omega_k$ and $\Delta\phi_k$ are the frequency and phase differences between signal field and the nearest peak. Responses from all the peaks mix up together though. Only the strongest beat signal from the response of the nearest peak is recognized and read out as long as f_r is set to be superior to the instantaneous bandwidth of the system. According to Eq. (21), the amplitude and the phase of the signal field can be directly read out from the beat note, but measurements are still needed to acquire the absolute frequency. So two MFCs denoted as MFC1 and MFC2 are utilized at different times to get two beat frequencies f_b and f_b'. A known offset frequency f_{offset} is fixed for both MFCs, and the repeating frequencies f_{r1} and f_{r2} are set to satisfy $\delta f_r = f_r - f_r' \ll f_r$. The absolute frequency of the signal f_s is written as follows:

$$f_s = f_{\text{offset}} + N \cdot f_r \pm f_b, \tag{22}$$

where N is the mode order number of MFC.

Due to the uncertainty of the sign before f_b, the exact value of f_s is calculated differently judging by the values of f_b and f_b'. With the assumption that $N \cdot \delta f_r \ll f_r/2$, the calculation of f_s is divided into two cases, which is appropriate for most occasions. Experiments are conducted with f_r being 4 MHz and 280 kHz respectively, and the outcome fits the applied frequency well as shown in Fig. 14. In the first case, a maximum comb span of 125 MHz is achieved, which far exceeds the number of the instantaneous bandwidth of a single-tone LO field system [143]. Since there is no need to adjust the LO field according to the signal, with two separating systems with different MFC fields, it is possible to realize real-time frequency measurement over a wide range. The MFC system also behaves well on receiving signals with 1 kHz bandwidth and phase recognition, which holds a high fidelity of 98%.

MFC system is capable of measuring the absolute frequency with a broad bandwidth compared to the single-tone LO field system and is a promising way to realize real-time measurement. The master equation is used to explain the results in Eq. (22). To get a more precise description, the Floquet method is expected to be applied to the MFC system. Due to the assumption that $N \cdot \delta f_r \ll f_r/2$, there are still cases that two different absolute frequencies exist simultaneously, so the method of MFC still demands a more sophisticated scheme to erase that uncertainty.

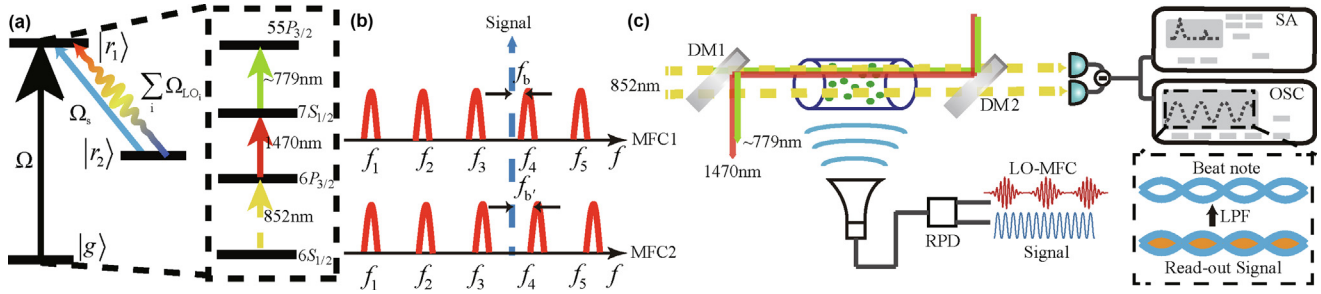

Fig. 13. (Color online) (a) The energy diagram of a Rydberg MFC spectrum. A laser drives the ground state $|g\rangle$ and the Rydberg state $|r_1\rangle$. For the experiment, three lasers are used to excite the atoms, as shown in the dashed box. A strong MFC field is set as a LO field (multicolor) and a signal field (blue) couples the two Rydberg states $|r_1\rangle$ and $|r_2\rangle$. (b) The signal beat (blue) with two MFCs (red). The beat-note frequencies are determined by the frequencies of the signal field and its nearest-neighbor MFC comb line. From the sum and difference of the $f_b \pm f_b'$, we calculate the mode-order number N of the nearest-neighbor MFC comb line. The absolute frequency of the signal field is obtained from the mode-order number and its offset from its nearest MFC frequency component. (c) The experimental setup. An 852-nm probe laser, a 1470-nm dressing laser, and a 779-nm coupling laser are used to excite and probe the Rydberg state. The MFC and signal fields are combined through a resistance power divider and transmitted to the vapor cell by a horn antenna. The beat-note signal is recorded and analyzed via an oscilloscope or a spectrum analyzer (SA) [142].

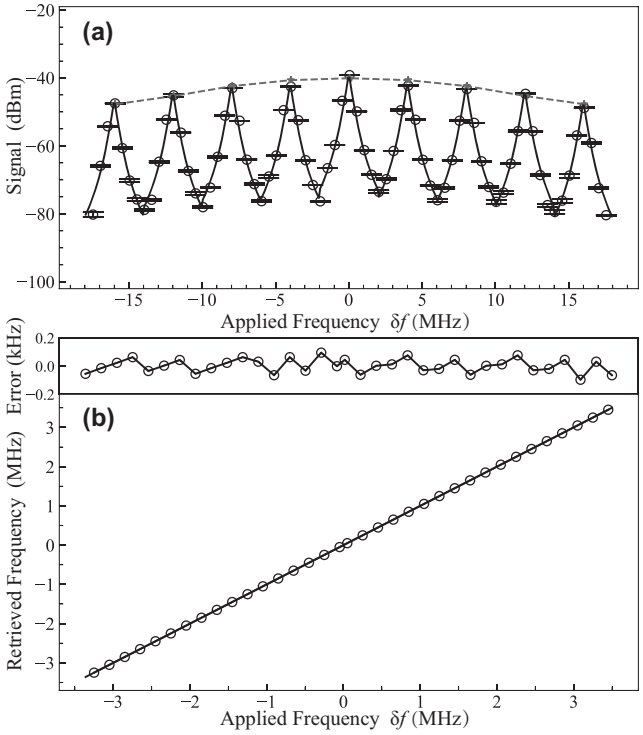

Fig. 14. (Color online) (a) The power of the beat note versus the signal-field frequency offset δf. The experimental data (black circles), the semi-steady-state theoretical result (red dashed line), and the time-dependent calculation results (black solid line) are shown. The beat note is recorded with a frequency separation of 500 kHz. Here, a nine-bin MFC field is used. (b) The retrieved frequency versus the signal-field frequency. Here, two 25-bin MFCs are used. The inset at the top shows the frequency error of approximately 100 Hz [142].

Shortly afterwards, a new self-heterodyne using an OFC was born [144], with a lowest detectable electromagnetic field of 66 μV cm^{-1} and sensitivities of 2.3 μV cm^{-1} Hz$^{-1/2}$. The scheme also enables real-time measurements because it eliminates the need for laser scanning.

7.3. Imaging

The high-resolution near-field characterization of microwave electric fields holds significant importance in the fields of chip-level electromagnetic compatibility (EMC) testing, high-voltage substation discharge detection, radio frequency identification (RFID) tags design and performance testing, etc. Hence high-resolution near-field imaging finds crucial applications in communication, national defense, and the biomedical sector. However, for near-field imaging with conventional antennas, the sensitivity is low due to the disturbances to the source fields caused by the metallic conductors of the antennas. The relatively large geometric dimensions of conventional antennas prevent them from achieving sub-wavelength spatial resolution in microwave electric field spatial measurements. It is a pending issue to improve the metrics of resolution maintaining high sensitivities.

The key element of an atomic sensor is a vapor cell made of dielectric materials. Compared to the metal antenna, the disturbance to the measured microwave electric field is thus greatly reduced. Furthermore, the imaging resolutions of atomic sensors are only limited by the size of the atom-light interaction region which is practically the laser widths rather than the size of the vapor cell containing atoms [145]. When the microwave irradiates the vapor cell, the standing wave pattern is generated inside the cell due to the internal multi-reflections of the waves from the inner cell walls. Considering the convenience of the experiment, generally, the vapor cell is placed on the translation stage. Moving the stage perpendicular to the propagation direction of the microwave realizes the relative motion of the vapor cell to the lasers interaction area. The resolution of 66 μm corresponding to $\sim \lambda/650$ at 6.9 GHz with the atomic sensor was first implemented [146] as shown in Fig. 15.

The spatial resolution ≈ 100 μm for the microwaves at 17.04 and 104.77 GHz is realized when measuring the electric field distribution inside the glass cylinder vapor cell using rubidium atoms [147]. The field distribution revealing information on both strength and polarization of the field is mapped for microwave at a frequency of 3.99 GHz. The deviation from the simulation of measurements taken with the atomic sensor is smaller than the metal probe, improving by 1.6 dB [148]. To enhance the robustness and avoid laser aberration in free space, fiber-integrated atomic vapor cells are introduced into the investigations [145,149–151].

Besides the depiction of radiation field patterns in the microwave regime, the imaging of Terahertz waves is also conducted. Downes et al. [152] showed that based on frequency conversion scheme, the efficient THz-to-optical conversion in atomic vapor cell was utilized for Terahertz imaging at frequency of 0.55 THz and a minimum detectable power of (190±30) fW s$^{-1/2}$ per (40×40) μm^2 pixel capable of video capture rate of 3 kHz was reached.

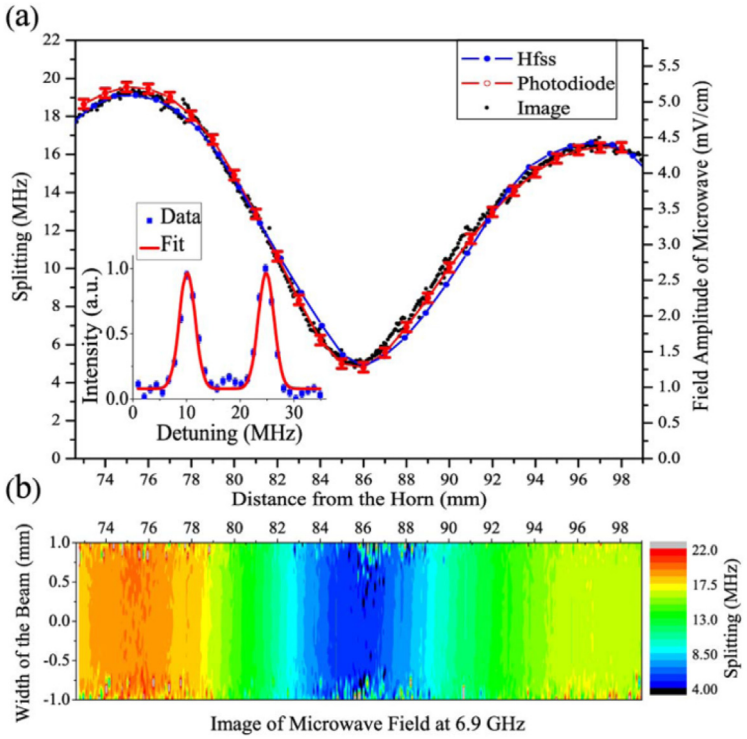

Fig. 15. (Color online) (a) Measurement of the EIT dark state splitting versus distance from the horn antenna. The theoretical FE calculation (blue), photodiode measurement (red), and image measurement data (black) are shown for a trace taken along the center line of the image. (b) 2D image of the MW electric field. The data are composed of 26 images with a step size of 1 mm in the direction along the cavity axis, *x*. In the transverse, *y* direction, a 2 mm cross-section with the zero point at the center of the probe beam is displayed. The error bars show the standard deviation between the photodiode and imaging measurements. The errors from fitting the data are small compared to variations in the measurements. The inset shows typical raw data (blue points) and the two Gaussian peak fit (red line).

8. Outlook

This review focuses on the progress of microwave sensing based on Rydberg atoms with respect to the theoretical models and experimental approaches in regard to key metrics such as sensitivities and bandwidths, together with the applications overview in the fields of metrology, communication, and imaging. However, there remains a lot of room for enhancement and improvement.

Sensitivity Most of the research mentioned above is in principle based on classical measurement strategies of which the sensitivities are proportional to the square root of atoms number participating in the sensing of microwaves ($\propto 1/\sqrt{N_{\text{atom}}}$) according to Eq. (11). Exploiting the non-classical light source would help beating the SQL related to photon shot noise such as squeezed light [153]. Improvement of sensitivity would also benefit from the suppression of the Doppler effect in the cold Rydberg atoms ensemble with atoms number comparable to that in room-temperature vapor cell [38]. The ultimate sensitivity of atomic microwave sensors based on uncorrelated atoms is limited. The authentic quantum-based atomic microwave sensing relies on the utilization of entangled collective Rydberg excitation states of which the sensitivity scales as $1/N_{\text{atom}}$ reaching the Heisenberg limit [154]. Sensitivity of 30 mV cm^{-1} Hz$^{-1/2}$ has been achieved by a single Rydberg atom with large angular momentum undergoing a non-classical evolution through Schrödinger-cat states [155]. The sensitivity would be greatly enhanced to be less than −200 dBm/Hz with increased atom number and limited by quantum projection noise.

Bandwidth There are intrinsic and external limitations on extending the instantaneous bandwidth such as steady states establishing and transit-time broadening. This review has introduced several research studies for the improvement of instantaneous bandwidth. The related high time-resolution pulse microwave recognition and retrieval are also of great importance in practice. The minimum 50 ns pulse duration with the sensitivity of about 240 nV cm^{-1} Hz$^{-1/2}$ has been reported [156]. The strong long-range interaction between Rydberg atoms would speed up the establishment of EIT steady state theoretically [157] which would be helpful for Rydberg atoms sensor to reach larger instantaneous bandwidth over 100 MHz in principle.

Precision Precision is the key metric in the field of SI traceable metrology which is of great significance for establishing standards for electric field both in weak and strong regimes in terms of intensity for varied frequencies, which is the foundation for modern science and technology and even more manufacturing industry. The primary limitation is induced by the vapor cell, specifically the standing-wave effect inside the cell. Early studies [94,95] showed that the geometry of vapor cell and wavelength of microwave affected the accuracy of the electric field measurement in the form of D/λ_{MW}, where D is the characteristic length of the vapor cell along the propagation direction of the microwave. In principle, the exploitation of metamaterials or metasurfaces may provide a solution to address the problems.

Nonetheless, the Rydberg sensor for microwave detection is a promising candidate in various application scenarios including radar, metrology, etc. The unprecedented theoretical sensitivity and universal instrument setup hold for the next generation of microwave detection and sensing.

Conflict of interest

The authors declare that they have no conflict of interest.

Acknowledgments

This work was supported by the National Key R&D Program of China (2022YFA1404000, 2021YFA1402004, and 2022YFA1405300), the National Natural Science Foundation of China (61827824, 61975104,12225405, U20A2074, U20A20218, 61525504, and 61435011), the Innovation Program for Quantum Science and Technology (2021ZD0301700), the Fund for Science and Technology on Electronic Information Control Laboratory and the Fund for Shanxi "331 Project" Key Subjects Construction, Bairen Project of Shanxi Province, China, the Anhui Initiative in Quantum Information Technologies (AHY020200), the Major Science and Technology Projects in Anhui Province (202203a13010001), National Research Foundation, Prime Ministers Office, Singapore and the Ministry of Education, Singapore under the Research Centres of Excellence programme.

Author contribution

Hao Zhang, Yu Ma, and Kaiyu Liao co-wrote the manuscript. Wenguang Yang and Zongkai Liu revised the figures and tables in the paper. Dongsheng Ding, Hui Yan, Wenhui Li, and Linjie Zhang conceived the idea and designed the structure of the paper. All of the authors contributed to the revision of the paper.

References

[1] Griffiths DJ. Introduction to Electrodynamics. 4th ed. Cambridge: Cambridge University Press; 2017. p. 210–66.
[2] Hertz H. Ueber strahlen electrischer kraft. Ann Phys 1889;272:769–83.
[3] Balanis CA. Antenna Theory: Analysis and Design. New York: Wiley-Interscience; 2005. p. 639–709.
[4] Johnson JB. Thermal agitation of electricity in conductors. Phys Rev 1928;32:97–109.
[5] Nyquist H. Thermal agitation of electric charge in conductors. Phys Rev 1928;32:110–3.
[6] Chu LJ. Physical limitations of omni-directional antennas. J Appl Phys 2004;19:1163–75.
[7] Wheeler H. Small antennas. IEEE Trans Antennas Propag 1975;23:462–9.
[8] Harrington RF. Effect of antenna size on gain, bandwidth, and efficiency. J Res Natl Bur Stand, Section D: Radio Propagation 1960;64D:1–12.
[9] Bothwell T, Kennedy CJ, Aeppli A, et al. Resolving the gravitational redshift across a millimetre-scale atomic sample. Nature 2022;602:420–4.
[10] Dang HB, Maloof AC, Romalis MV. Ultrahigh sensitivity magnetic field and magnetization measurements with an atomic magnetometer. Appl Phys Lett 2010;97:151110.
[11] Tiesinga E, Mohr PJ, Newell DB, et al. Codata recommended values of the fundamental physical constants: 2018. Rev Mod Phys 2021;93:025010.
[12] Šibalic N, Pritchard J, Adams C, et al. Arc: An open-source library for calculating properties of alkali rydberg atoms. Comput Phys Commun 2017;220:319–31.
[13] Gallagher TF, Humphrey LM, Hill RM, et al. Resolution of $|m_l|$ and $|m_j|$ levels in the electric field ionization of highly excited d states of na. Phys Rev Lett 1976;37:1465–7.
[14] Gallagher TF, Humphrey LM, Cooke WE, et al. Field ionization of highly excited states of sodium. Phys Rev A 1977;16:1098–108.
[15] Mudrich M, Zahzam N, Vogt T, et al. Back and forth transfer and coherent coupling in a cold rydberg dipole gas. Phys Rev Lett 2005;95:233002.
[16] Vogt T, Viteau M, Zhao J, et al. Dipole blockade at förster resonances in high resolution laser excitation of rydberg states of cesium atoms. Phys Rev Lett 2006;97:083003.
[17] Vogt T, Viteau M, Chotia A, et al. Electric-field induced dipole blockade with rydberg atoms. Phys Rev Lett 2007;99:073002.
[18] Zhang H, Wang L, Zhang L, et al. Stark-induced l-mixing interferences in ultracold cesium rydberg atoms. Phys Rev A 2013;87:033405.
[19] Wang L, Zhang H, Zhang L, et al. Dipolar rydberg-atom gas prepared by adiabatic passage through an avoided crossing. New J Phys 2015;17:063011.
[20] Wang L, Zhang H, Zhang L, et al. Atom-interferometric measurement of stark level splittings. Phys Rev A 2015;92:033619.
[21] Boller KJ, Imamolu A, Harris SE. Observation of electromagnetically induced transparency. Phys Rev Lett 1991;66:2593–6.
[22] Harris SE, Field JE, Imamolu A. Nonlinear optical processes using electromagnetically induced transparency. Phys Rev Lett 1990;64:1107–10.
[23] Fleischhauer M, Imamoglu A, Marangos JP. Electromagnetically induced transparency: Optics in coherent media. Rev Mod Phys 2005;77:633–73.
[24] Mohapatra AK, Jackson TR, Adams CS. Coherent optical detection of highly excited rydberg states using electromagnetically induced transparency. Phys Rev Lett 2007;98:113003.
[25] Zhao J, Zhu X, Zhang L, et al. High sensitivity spectroscopy of cesium Rydberg atoms using electromagnetically induced transparency. Opt Exp 2009;17:15821–6.
[26] Pritchard JD, Maxwell D, Gauguet A, et al. Cooperative atom-light interaction in a blockaded rydberg ensemble. Phys Rev Lett 2010;105:193603.
[27] Maxwell D, Szwer DJ, Paredes-Barato D, et al. Storage and control of optical photons using rydberg polaritons. Phys Rev Lett 2013;110:103001.
[28] Abel RP, Mohapatra AK, Bason MG, et al. Laser frequency stabilization to excited state transitions using electromagnetically induced transparency in a cascade system. Appl Phys Lett 2009;94:071107.
[29] Jiao Y, Li J, Wang L, et al. Laser frequency locking based on Rydberg electromagnetically induced transparency. Chin Phys B 2016;25:053201.
[30] Li W, Tanner PJ, Gallagher TF. Dipole-dipole excitation and ionization in an ultracold gas of Rydberg atoms. Phys Rev Lett 2005;94:173001.
[31] Han J, Gallagher TF. Millimeter-wave rubidium rydberg van der Waals spectroscopy. Phys Rev A 2009;79:053409.
[32] Li W, Mourachko I, Noel MW, et al. Millimeter-wave spectroscopy of cold Rb Rydberg atoms in a magneto-optical trap: Quantum defects of the ns, np, and nd series. Phys Rev A 2003;67:052502.
[33] Han J, Jamil Y, Norum DVL, et al. Rb nf quantum defects from millimeter-wave spectroscopy of cold ^{85}Rb rydberg atoms. Phys Rev A 2006;74:054502.
[34] Moore K, Duspayev A, Cardman R, et al. Measurement of the Rb g-series quantum defect using two-photon microwave spectroscopy. Phys Rev A 2020;102:062817.
[35] Zhou Y, Grimes DD, Barnum TJ, et al. Direct detection of Rydberg–Rydberg millimeter-wave transitions in a buffer gas cooled molecular beam. Chem Phys Lett 2015;640:124–36.
[36] Department A. Electronic Warfare and Radar Systems Engineering Handbook. Naval Air Warfare Center Weapons Division; 2013.
[37] Fan H, Kumar S, Sedlacek J, et al. Atom based RF electric field sensing. J Phys B: At Mol Opt Phys 2015;48:202001.
[38] Schmidt M, Bohaichuk SM, Venu V, et al. Rydberg atom-based radio frequency sensors: Amplitude regime sensing. arXiv: 230700121; 2023.
[39] Cui Y, Jia FD, Hao JH, et al. Extending bandwidth sensitivity of Rydberg-atom-based microwave electrometry using an auxiliary microwave field. Phys Rev A 2023;107:043102.
[40] Biercuk MJ, Uys H, Britton JW, et al. Ultrasensitive detection of force and displacement using trapped ions. Nat Nanotechnol 2010;5:646–50.
[41] Meyer DH, Castillo ZA, Cox KC, et al. Assessment of rydberg atoms for wideband electric field sensing. J Phys B: At Mol Opt Phys 2020;53:034001.
[42] Toney JE, Tarditi AG, Pontius P, et al. Detection of energized structures with an electro-optic electric field sensor. IEEE sensors J 2014;14:1364–9.
[43] Zhao J, Zhang H, Feng Z, et al. Measurement of polarizability of cesium nd state in magneto-optical trap. J Phys Soc Jpn 2011;80:034303.
[44] Bai J, Bai S, Han X, et al. Precise measurements of polarizabilities of cesium ns Rydberg states in an ultra-cold atomic ensemble. New J Phys 2020;22:093032.
[45] Osterwalder A, Merkt F. Using high Rydberg states as electric field sensors. Phys Rev Lett 1999;82:1831–4.
[46] Sedlacek JA. Microwave and surface electrometry with Rydberg atoms Dissertation for Doctoral Degree. Norman: University of Oklahoma; 2016.
[47] Garofalini SH, Zirl DM. Onset of alkali adsorption on the vitreous silica surface. J Vac Sci Technol A 1988;6:975–81.
[48] Ma L, Paradis E, Raithel G. Dc electric fields in electrode-free glass vapor cell by photoillumination. Opt Express 2020;28:3676–85.
[49] Jau YY, Carter T. Vapor-cell-based atomic electrometry for detection frequencies below 1 kHz. Phys Rev Appl 2020;13:054034.
[50] Lee ES, Cho S, Lyeo HK, et al. Seebeck effect at the atomic scale. Phys Rev Lett 2014;112:136601.
[51] Muray JJ. Photoelectric effect induced by high intensity laser light beam in quartz and borosilicate glass; 2018.
[52] Gallagher TF Rydberg. Atoms. Cambridge Monographs on Atomic, Molecular and Chemical Physics. Cambridge: Cambridge University Press; 1994. p. 195–250.
[53] Wang X, He J, Bai J, et al. Rydberg level shift due to the electric field generated by Rydberg atom collision induced ionization in cesium atomic ensemble. Appl Sci 2020;10:5646.
[54] Anderson DA, Raithel G, Simons M, et al. Quantum-optical spectroscopy for plasma electric field measurements and diagnostics. arXiv: 1712.08717, 2017.
[55] Jiao Y, Han X, Yang Z, et al. Spectroscopy of cesium Rydberg atoms in strong radio-frequency fields. Phys Rev A 2016;94:023832.
[56] Miller SA, Anderson DA, Raithel G. Radio-frequency-modulated Rydberg states in a vapor cell. New J Phys 2016;18:053017.
[57] Anderson DA, Schwarzkopf A, Miller SA, et al. Two-photon microwave transitions and strong-field effects in a room-temperature Rydberg-atom gas. Phys Rev A 2014;90:043419.
[58] Anderson DA, Miller SA, Raithel G, et al. Optical measurements of strong microwave fields with Rydberg atoms in a vapor cell. Phys Rev Appl 2016;5:034003.
[59] Anderson DA, Paradis E, Raithel G, et al. High-resolution antenna near-field imaging and sub-thz measurements with a small atomic vapor-cell sensing

element. In: *Proceedings of the 2018 11th Global Symposium on Millimeter Waves (GSMM)*. 2018, p. 1–3.
[60] Anderson DA, Paradis EG, Raithel G. A vapor-cell atomic sensor for radio-frequency field detection using a polarization-selective field enhancement resonator. Appl Phys Lett 2018;113:073501.
[61] Paradis E, Raithel G, Anderson DA. Atomic measurements of high-intensity VHF-band radio-frequency fields with a rydberg vapor-cell detector. Phys Rev A 2019;100:013420.
[62] Holloway CL, Prajapati N, Sherman JA, et al. Electromagnetically induced transparency based rydberg-atom sensor for traceable voltage measurements. AVS Quantum Sci 2022;4:034401.
[63] Ma L, Viray MA, Anderson DA, et al. Measurement of dc and ac electric fields inside an atomic vapor cell with wall-integrated electrodes. Phys Rev Appl 2022;18:024001.
[64] Prajapati N, Bhusal N, Rotunno AP, et al. Sensitivity comparison of two-photon vs three-photon rydberg electrometry. J Appl Phys 2023;134:023101.
[65] Sedlacek JA, Schwettmann A, Kübler H, et al. Microwave electrometry with rydberg atoms in a vapour cell using bright atomic resonances. Nat Phys 2012;8:819–24.
[66] Sedlacek JA, Schwettmann A, Kübler H, et al. Atom-based vector microwave electrometry using rubidium rydberg atoms in a vapor cell. Phys Rev Lett 2013;111:063001.
[67] Gordon JA, Holloway CL, Schwarzkopf A, et al. Millimeter wave detection via autler-townes splitting in rubidium Rydberg atomsa. Appl Phys Lett 2014;105:024104.
[68] Holloway CL, Gordon JA, Jefferts S, et al. Broadband rydberg atom-based electric-field probe for Si-traceable, self-calibrated measurements. IEEE Trans Antennas Propag 2014;62:6169–82.
[69] Simons MT, Gordon JA, Holloway CL. Simultaneous use of Cs and Rb Rydberg atoms for dipole moment assessment and RF electric field measurements via electromagnetically induced transparency. J Appl Phys 2016;120:123103.
[70] Holloway CL, Simons MT, Haddab AH, et al. A "real-time" guitar recording using rydberg atoms and electromagnetically induced transparency: Quantum physics meets music. AIP Adv 2019;9:065110.
[71] Skolnik MI. Introduction to Radar Systems. 2nd ed. Singapore: McGraw-Hill book company; 1980.
[72] Degen CL, Reinhard F, Cappellaro P. Quantum sensing. Rev Mod Phys 2017;89:035002.
[73] Kitching J, Knappe S, Donley EA. Atomic sensors—a review. IEEE Sensors J 2011;11:1749–58.
[74] Itano WM, Bergquist JC, Bollinger JJ, et al. Quantum projection noise: Population fluctuations in two-level systems. Phys Rev A 1993;47:3554–70.
[75] Meyer DH, O'Brien C, Fahey DP, et al. Optimal atomic quantum sensing using electromagnetically-induced-transparency readout. Phys Rev A 2021;104:043103.
[76] Simons MT, Gordon JA, Holloway CL, et al. Using frequency detuning to improve the sensitivity of electric field measurements via electromagnetically induced transparency and autler-townes splitting in rydberg atoms. Appl Phys Lett 2016;108:174101.
[77] Zhang L, Jia Y, Jing M, et al. Detuning radio-frequency electrometry using rydberg atoms in a room-temperature vapor cell. Laser Phys 2019;29:035701.
[78] Kumar S, Fan H, Kubler H, et al. Atom-based sensing of weak radio frequency electric fields using homodyne readout. Sci Rep 2017;7:42981.
[79] Yang W, Jing M, Zhang H, et al. Enhancing the sensitivity of atom-based microwave-field electrometry using a mach-zehnder interferometer. Phys Rev Appl 2023;19:064021.
[80] Kumar S, Fan H, Kübler H, et al. Rydberg-atom based radio-frequency electrometry using frequency modulation spectroscopy in room temperature vapor cells. Opt Express 2017;25:8625–37.
[81] Cai M, Xu Z, You S, et al. Sensitivity improvement and determination of rydberg atom-based microwave sensor. Photonics 2022;9:250.
[82] Cai M, You S, Zhang S, et al. Sensitivity extension of atom-based amplitude-modulation microwave electrometry via high rydberg states. Appl Phys Lett 2023;122:161103.
[83] Li S, Yuan J, Wang L. Improvement of microwave electric field measurement sensitivity via multi-carrier modulation in rydberg atoms. Appl Sci 2020;10:8110.
[84] Jia F, Yu Y, Liu X, et al. Dispersive microwave electrometry using zeeman frequency modulation spectroscopy of electromagnetically induced transparency in rydberg atoms. Appl Opt 2020;59:8253–8.
[85] Zhou F, Jia F, Liu X, et al. Improving the spectral resolution and measurement range of quantum microwave electrometry by cold rydberg atoms. J Phys B: At Mol Opt Phys 2023;56:025501.
[86] Liao KY, Tu HT, Yang SZ, et al. Microwave electrometry via electromagnetically induced absorption in cold rydberg atoms. Phys Rev A 2020;101:053432.
[87] Sheng J, Chao Y, Kumar S, et al. Intracavity rydberg-atom electromagnetically induced transparency using a high-finesse optical cavity. Phys Rev A 2017;96:033813.
[88] Peng Y, Wang J, Yang A, et al. Cavity-enhanced microwave electric field measurement using rydberg atoms. J Opt Soc Am B 2018;35:2272–7.
[89] Peng YD, Wang JL, Li C, et al. Enhanced microwave electrometry with intracavity anomalous dispersion in rydberg atoms. Opt Quantum Electron 2020;52:120.
[90] Yang A, Zhou W, Zhao S, et al. Enhanced measurement of microwave electric fields with collective rabi splitting. J Opt Soc Am B 2020;37:1664–9.
[91] Holloway CL, Simons MT, Gordon JA, et al. Electric field metrology for si traceability: Systematic measurement uncertainties in electromagnetically induced transparency in atomic vapor. J Appl Phys 2017;121:233106.
[92] Chopinaud A, Pritchard JD. Optimal state choice for rydberg-atom microwave sensors. Phys Rev Appl 2021;16:024008.
[93] Hao L, Xue Y, Fan J, et al. Nonlinearity of microwave electric field coupled rydberg electromagnetically induced transparency and autler-townes splitting. Appl Sci 2019;9:1720.
[94] Fan H, Kumar S, Sheng J, et al. Effect of vapor-cell geometry on rydberg-atom-based measurements of radio-frequency electric fields. Phys Rev Appl 2015;4:044015.
[95] Zhang L, Liu J, Jia Y, et al. Vapor cell geometry effect on rydberg atom-based microwave electric field measurement. Chin Phys B 2018;27:033201.
[96] Song Z, Zhang W, Wu Q, et al. Field distortion and optimization of a vapor cell in rydberg atom-based radio-frequency electric field measurement. Sensors 2018;18:3205.
[97] Simons MT, Kautz MD, Gordon JA, et al. Uncertainties in rydberg atom-based RF e-field measurements. In: *Proceedings of the International Symposium on Electromagnetic Compatibility (EMC EUROPE)*. 2018; 376–380.
[98] Simons MT, Kautz MD, Holloway CL, et al. Electromagnetically induced transparency (EIT) and autler-townes (AT) splitting in the presence of band-limited white gaussian noise. J Appl Phys 2018;123:203105.
[99] Carr C, Tanasittikosol M, Sargsyan A, et al. Three-photon electromagnetically induced transparency using rydberg states. Opt Lett 2012;37:3858–60.
[100] Shaffer J, Kübler H. A read-out enhancement for microwave electric field sensing with rydberg atoms. SPIE Photonics Europe 2018;10674:106740C.
[101] Ripka F, Amarloo H, Erskine J, et al. Application-driven problems in rydberg atom electrometry. SPIE OPTO 2021;11700:117002Y.
[102] Shaffer JP, Ripka F, Liu C, et al. Rydberg atom-based radio frequency electrometry: Enhancement of the self-calibrated autler-townes sensing mode. In: *Proceedings of the 2021 IEEE Conference on Antenna Measurements & Applications (CAMA)*. 2021, p. 226–229.
[103] Liu B, Zhang LH, Liu ZK, et al. Highly sensitive measurement of a megahertz rf electric field with a rydberg-atom sensor. Phys Rev Appl 2022;18:014045.
[104] Gordon JA, Simons MT, Haddab AH, et al. Weak electric-field detection with sub-1 Hz resolution at radio frequencies using a rydberg atom-based mixer. AIP Adv 2019;9:045030.
[105] Jing M, Hu Y, Ma J, et al. Atomic superheterodyne receiver based on microwave-dressed rydberg spectroscopy. Nat Phys 2020;16:911–5.
[106] Yan Y, Yuan J, Zhang L, et al. Three-dimensional location system based on an l-shaped array of rydberg atomic receivers. Opt Lett 2023;48:3945–8.
[107] Prajapati N, Robinson AK, Berweger S, et al. Enhancement of electromagnetically induced transparency based rydberg-atom electrometry through population repumping. Appl Phys Lett 2021;119:214001.
[108] You SH, Cai MH, Zhang SS, et al. Microwave-field sensing via electromagnetically induced absorption of Rb irradiated by three-color infrared lasers. Opt Express 2022;30:16619–29.
[109] Hu J, Li H, Song R, et al. Continuously tunable radio frequency electrometry with rydberg atoms. Appl Phys Lett 2022;121:014002.
[110] Li H, Hu J, Bai J, et al. Rydberg atom-based am receiver with a weak continuous frequency carrier. Opt Express 2022;30:13522–9.
[111] Zhang P, Jing M, Wang Z, et al. Quantum scaling atomic superheterodyne receiver. EPJ Quantum Technol 2023;10:39.
[112] Wang Z, Jing M, Zhang P, et al. Noise analysis of the atomic superheterodyne receiver based on flat-top laser beams. Opt Express 2023;31:19909–17.
[113] Simons MT, Haddab AH, Gordon JA, et al. A rydberg atom-based mixer: Measuring the phase of a radio frequency wave. Appl Phys Lett 2019;114:114101.
[114] Robinson AK, Prajapati N, Senic D, et al. Determining the angle-of-arrival of a radio-frequency source with a rydberg atom-based sensor. Appl Phys Lett 2021;118:114001.
[115] Anderson DA, Sapiro RE, Gonçalves LF, et al. Optical radio-frequency phase measurement with an internal-state rydberg atom interferometer. Phys Rev Appl 2022;17:044020.
[116] Yang B, Yan Y, Li X, et al. Highly sensitive microwave electrometry with enhanced instantaneous bandwidth. Phys Rev Appl 2024;21:L031003.
[117] Simons MT, Artusio-Glimpse AB, Holloway CL, et al. Continuous radio-frequency electric-field detection through adjacent rydberg resonance tuning. Phys Rev A 2021;104:032824.
[118] Liu XH, Liao KY, Zhang ZX, et al. Continuous-frequency microwave heterodyne detection in an atomic vapor cell. Phys Rev Appl 2022;18:054003.
[119] Han J, Vogt T, Gross C, et al. Coherent microwave-to-optical conversion via six-wave mixing in rydberg atoms. Phys Rev Lett 2018;120:093201.
[120] Tu HT, Liao KY, Zhang ZX, et al. High-efficiency coherent microwave-to-optics conversion via off-resonant scattering. Nat Photon 2022;16:291–6.

[121] Kiffner M, Feizpour A, Kaczmarek K, et al. Two-way interconversion of millimeter-wave and optical fields in rydberg gases. New J Phys 2016;18:093030.
[122] Kumar A, Suleymanzade A, Stone M, et al. Quantum-enabled millimetre wave to optical transduction using neutral atoms. Nature 2023;615:614–9.
[123] Borówka S, Pylypenko U, Mazelanik M, et al. Continuous wideband microwave-to-optical converter based on room-temperature rydberg atoms. Nat Photon 2023;18:32–8.
[124] Ding DS, Liu ZK, Shi BS, et al. Enhanced metrology at the critical point of a many-body rydberg atomic system. Nat Phys 2022;18:1447–52.
[125] Holloway CL, Simons MT, Kautz MD, et al. A quantum-based power standard: Using rydberg atoms for a SI-traceable radio-frequency power measurement technique in rectangular waveguides. Appl Phys Lett 2018;113:094101.
[126] Song Z, Feng Z, Liu X, et al. Quantum-based determination of antenna finite range gain by using rydberg atoms. IEEE Antennas Wireless Propag Lett 2017;16:1589–92.
[127] Cox KC, Meyer DH, Fatemi FK, et al. Quantum-limited atomic receiver in the electrically small regime. Phys Rev Lett 2018;121:110502.
[128] Meyer DH, Cox KC, Fatemi FK, et al. Digital communication with rydberg atoms and amplitude-modulated microwave fields. Appl Phys Lett 2018;112:211108.
[129] Jiao Y, Han X, Fan J, et al. Atom-based receiver for amplitude-modulated baseband signals in high-frequency radio communication. Appl Phys Express 2019;12:126002.
[130] Song Z, Liu H, Liu X, et al. Rydberg-atom-based digital communication using a continuously tunable radio-frequency carrier. Opt Express 2019;27:8848–57.
[131] Holloway CL, Simons MT, Gordon JA, et al. Detecting and receiving phase-modulated signals with a rydberg atom-based receiver. IEEE Antennas Wireless Propag Lett 2019;18:1853–7.
[132] Menchetti M, Bussey LW, Gilks D, et al. Digitally encoded RF to optical data transfer using excited Rb without the use of a local oscillator. J Appl Phys 2023;133:014401.
[133] Anderson DA, Sapiro RE, Raithel G. An atomic receiver for AM and FM radio communication. IEEE Trans Antennas Propag 2021;69:2455–62.
[134] Zou H, Song Z, Mu H, et al. Atomic receiver by utilizing multiple radio-frequency coupling at rydberg states of rubidium. Appl Sci 2020;10:1346.
[135] Cai Y, Shi S, Zhou Y, et al. High-sensitivity rydberg-atom-based phase-modulation receiver for frequency-division-multiplexing communication. Phys Rev Appl 2023;19:044079.
[136] Otto JS, Hunter MK, Kjærgaard N, et al. Data capacity scaling of a distributed rydberg atomic receiver array. J Appl Phys 2021;129:154503.
[137] Prajapati N, Rotunno AP, Berweger S, et al. Tv and video game streaming with a quantum receiver: A study on a rydberg atom-based receiver's bandwidth and reception clarity. AVS Quantum Sci 2022;4:035001.
[138] Meyer DH, Hill JC, Kunz PD, et al. Simultaneous multiband demodulation using a rydberg atomic sensor. Phys Rev Appl 2023;19:014025.
[139] Knarr SH, Bucklew VG, Langston J, et al. Spatiotemporal multiplexed rydberg receiver. IEEE Trans Quantum Eng 2023;4:1–8.
[140] Fortier T, Baumann E. 20 years of developments in optical frequency comb technology and applications. Commun Phys 2019;2:153.
[141] Diddams SA, Jones DJ, Ye J, et al. Direct link between microwave and optical frequencies with a 300 thz femtosecond laser comb. Phys Rev Lett 2000;84:5102.
[142] Zhang LH, Liu ZK, Liu B, et al. Rydberg microwave-frequency-comb spectrometer. Phys Rev Appl 2022;18:014033.
[143] Meyer DH, Kunz PD, Cox KC. Waveguide-coupled rydberg spectrum analyzer from 0 to 20 GHz. Phys Rev Appl 2021;15:014053.
[144] Dixon K, Nickerson K, Booth DW, et al. Rydberg-atom-based electrometry using a self-heterodyne frequency-comb readout and preparation scheme. Phys Rev Appl 2023;19:034078.
[145] Holloway CL, Simons MT, Gordon JA, et al. Atom-based rf electric field metrology: From self-calibrated measurements to subwavelength and near-field imaging. IEEE Trans Electromagn Compat 2017;59:717–28.
[146] Fan HQ, Kumar S, Daschner R, et al. Subwavelength microwave electric-field imaging using rydberg atoms inside atomic vapor cells. Opt Lett 2014;39:3030–3.
[147] Holloway CL, Gordon JA, Schwarzkopf A, et al. Sub-wavelength imaging and field mapping via electromagnetically induced transparency and autler-townes splitting in rydberg atoms. Appl Phys Lett 2014;104:244102.
[148] Bai J, Fan J, Hao L, et al. Measurement of the near field distribution of a microwave horn using a resonant atomic probe. Appl Sci 2019;9:4895.
[149] Holloway CL, Simons MT, Kautz M, et al. Development and applications of a fiber-coupled atom-based electric field probe. In: *Proceedings of the 2018 International Symposium on Electromagnetic Compatibility (EMC EUROPE)*. 2018, p. 381–385.
[150] Simons MT, Gordon JA, Holloway CL. Fiber-coupled vapor cell for a portable rydberg atom-based radio frequency electric field sensor. Appl Opt 2018;57:6456–60.
[151] Mao R, Lin Y, Yang K, et al. A high-efficiency fiber-coupled rydberg-atom integrated probe and its imaging applications. IEEE Antennas Wireless Propag Lett 2023;22:352–6.
[152] Downes LA, MacKellar AR, Whiting DJ, et al. Full-field terahertz imaging at kilohertz frame rates using atomic vapor. Phys Rev X 2020;10:011027.
[153] Prajapati N, Niu Z, Novikova I. Quantum-enhanced two-photon spectroscopy using two-mode squeezed light. Opt Lett 2021;46:1800–3.
[154] Giovannetti V, Lloyd S, Maccone L. Quantum-enhanced measurements: Beating the standard quantum limit. Science 2004;306:1330–6.
[155] Facon A, Dietsche EK, Grosso D, et al. A sensitive electrometer based on a rydberg atom in a schrodinger-cat state. Nature 2016;535:262–5.
[156] Bohaichuk SM, Booth D, Nickerson K, et al. Origins of rydberg-atom electrometer transient response and its impact on radio-frequency pulse sensing. Phys Rev Appl 2022;18:034030.
[157] Zhang Q, Bai Z, Huang G. Fast-responding property of electromagnetically induced transparency in rydberg atoms. Phys Rev A 2018;97:043821.

Hao Zhang received his B.S. degree (2006) in Sichuan University and Ph.D. degree (2014) in Shanxi University under the supervision of Prof. Suotang Jia. He is currently an associate professor at Institute of Laser Spectroscopy in Shanxi University. His research interest focuses on the precision measurement of microwave based on Rydberg atoms and quantum simulation with cold atoms as well as quantum optics phenomenon related to Rydberg physics.

Yu Ma received his B.S. degree (2023) in University of Science and Technology of China (USTC). Now he is studying for a master's degree in USTC under the guidance of Prof. Dongsheng Ding. He is interested and working on quantum sensing based on Rydberg atoms at room temperature, trying to make it an advanced alternative among microwave sensing methods.

Kai-Yu Liao received his B.S. degree (2010) in Xi'an University of Technology and Ph.D. degree (2016) in South China Normal University. Now he is a associate professor at School of Physics of South China Normal University. He is currently focusing on experimental quantum precision measurement, quantum physics and technology towards microwave antenna based on Rydberg atoms.

Dong-Sheng Ding received the Ph.D. degree in Physics from the USTC in 2015. He is now a professor at the USTC. He is mainly engaged in quantum storage and quantum communication based on cold atomic ensembles, quantum computing and quantum simulation based on Rydberg atoms and quantum sensing based on Rydberg atoms.

Hui Yan received his B.S. degree (2004) from Wuhan University and Ph.D. degree (2009) from Wuhan Institute of Physics and Mathematics of Chinese Academy of Sciences. Now he is a professor at School of Physics of South China Normal University. His research interest includes the quantum optics, quantum computation and quantum manipulation with cold atoms, and currently, the hybrid superconductor-atom quantum interface.

Wenhui Li has received her Ph.D. degree from the University of Virginia under the supervision of Prof. Gallagher. In 2009, she was faculty of Centre for Quantum Technologies at the National University of Singapore. She is currently a Professor at the Institute of Opto-Electronics at Shanxi University. Her research focuses on Rydberg-atom based quantum physics and related quantum technologies, including quantum measurements, quantum simulation of many-body systems, nonlinear processes, hybrid quantum systems, etc.

Linjie Zhang received his B.S. degree (1996) and Ph.D. degree (2010) in Shanxi University under the supervision of Prof. Suotang Jia. He is currently a full professor at Institute of Laser Spectroscopy in Shanxi University. His research interest focuses on the precision measurement with Rydberg atoms and quantum simulation and quantum optics phenomenon related to Rydberg physics.